UILU-ENG 85-3601

Report No. 117

A COMPARISON OF METHODS FOR PREDICTING WELDMENT FATIGUE LIFE UNDER VARIABLE LOAD HISTORIES

by

J.-Y. Yung and F. V. Lawrence
Departments of Metallurgy and Civil Engineering

A Report of the

MATERIALS ENGINEERING - MECHANICAL BEHAVIOR

College of Engineering, University of Illinois at Urbana-Champaign

January 1985

A COMPARISON OF METHODS FOR PREDICTING WELDMENT FATIGUE LIFE UNDER VARIABLE LOADING HISTORIES

ABSTRACT

Cruciform joints were fatigue tested under SAE Bracket variable loading history. Tube-to-plate welds were fatigue tested under bending and torsion loading conditions. Fatigue test results were compared with predictions made using the total fatigue life model which predicts the total fatigue life of weldments by combining estimates of fatigue crack initiation life and the fatigue crack propagation life. The comparisons of the total fatigue life model and other prediction models were also made.

ACKNOWLEDGEMENTS

This study was principally supported by the University of Illinois Fracture Control Program which is funded by a consortium of midwest industries.

Grateful acknowledgements are made to Mr. R. A. Testin of General Motors Electro-Motive Division, Mr. B.N. Babu of Caterpillar Tractor Co., and Mr. D. W. Prine of GARD, INC. for providing specimens, and to Dr. D. H. Sherman and Mr. W. P. Evans of Caterpillar Tractor Co. for measuring the residual stresses. Thanks are also extended to Professor D. F. Socie of the Department of Mechanical Engineering for his valuable discussions.

Ms. Claudia Petrie is particularly thanked for typing the manuscript.

TABLE OF CONTENTS

LIST OF SYMBOLS

a, a_i, a_f	crack length, initial crack length, final crack length
b	fatigue strength exponent
C	fatigue crack growth coefficient; also, S-N curve coefficient
c	fatigue ductility exponent; also, half length of lack of penetration and length of major axis of elliptical crack
D_i, D_{block}	fatigue damage per cycle and per block, respectively
E	Young's modulus
F	function of residual stress distribution
K'	cyclic strength coefficient
K_f, K_{fmax}	fatigue notch factor and maximum fatigue notch factor
K_t	elastic stress concentration factor
K_{max}^{rms}, K_{min}^{rms}	maximum and minimum root mean square stress intensity factor
K_r	stress intensity factor due to residual stress
ΔK	stress intensity factor range
ΔK_{rms}	root mean square stress intensity factor range
ℓ	leg length of weld
m	S-N curve slope
M_s, M_t, M_k	magnification factor for free surface, width and stress gradient
N_f	cycles to failure
$2N_{fi}$	reversals to failure
N_i, N_{fi}	cycles to failure at ith amplitude
N_T, N_I, N_p	total, initiation and propagation fatigue life

n	fatigue crack growth exponent
n'	cyclic strain hardening exponent
n_i	cycles at ith amplitude
Q, Θ_o	crack shape factor for an elliptical crack
R	stress ratio
R_F	reliability factor
r	notch root radius
S, S_a, S_o $S_{rms_{max}}$, $S_{rms_{min}}$	remote stress, amplitude of remote stress, remote mean stress and root mean square of maximum and minimum stress
S_o^B	gripping bending stress
S_u	ultimate tensile stress
t	plate thickness
w	specimen width
Y	geometry factor
α, β, λ	geometry coefficients for elastic stress concentration factor
ε, $\Delta\varepsilon$	local strain and local strain range
ε_f'	fatigue ductility coefficient
ε_n	strain normal to the crack
Γ	gamma function

σ, $\Delta\sigma$, σ_a, σ_o, σ_r	local stress, local stress range, local stress amplitude mean stress and residual stress
σ'_f	fatigue strength coefficient
θ	flank angle of welds
ξ	random load factor
Ω_N	total uncertainty

I. INTRODUCTION

1. Predicting the Fatigue Resistance of Welds under Variable Loading Histories

During the last half-century, numerous laboratory fatigue tests have been conducted on weldments, the great majority of which have been carried out under simple, constant amplitude loading. In service, welded structures are subjected to complex variable loads. Constant amplitude fatigue test results have been used as a basis for predicting the fatigue strength of weldments subjected to variable loadings. In the current design practice, the Palmgren-Miner's linear damage rule (or commonly 'Miner's rule') is recommended for the cumulative damage calculation. However, for variable load histories, stress cycles below the constant amplitude fatigue limit might cause damage. Neglecting this contribution to damage will introduce unconservatism in fatigue life prediction using the Miner's rule. Nevertheless, the linear cumulative damage has been shown to be acceptably accurate for welds subjected to a pseudo-constant amplitude stress spectrum without periodic overloads.

In an attempt to improve the utility of the S-N-diagram-based life prediction methods, several models have been proposed: Munse [1] proposed a fatigue design criterion using statistics and reliability; Gurney [2] proposed an empirical model based on test results; Joehnk and Zwerneman [3] introduced a nonlinear cumulative damage model.

Fatigue testing is expensive and time-consuming, especially for full-scale weldments. Typical S-N diagrams exhibit a large amount of scatter resulting mainly from variations in the stress state and weld geometry. In order to make fatigue predictions for different weld geometries and load histories, analytical models are needed. Maddox [4] predicted the fatigue

crack propagation life of welds under variable loading histories using the linear fracture mechanics. A simple root-mean-square (RMS) model was proposed later by Barsom [5]. Neither of the S-N diagram methods or the fracture mechanics models consider the effects of mean stress and residual stresses. Moreover, the fracture mechanics models neglect the fatigue crack initation phase. In order to account for these effects and include the fatigue crack initiation life, Lawrence et al. [6] have developed a total fatigue life model (I-P model) to predict the fatigue resistance of welds subjected to variable loading. The total fatigue life model will be discussed below.

2. The Total Fatigue Life Model

The total fatigue life model predicts the total fatigue life (N_T) of weldments by combining estimates of the fatigue crack initiation life (N_I) and the fatigue crack propagation life (N_P):

$$N_T = N_I + N_P \tag{1}$$

where N_I is the fatigue life devoted to the initiation of fatigue cracks and their early growth and coalescence into a dominant fatigue crack, N_P involves the propagation of the dominant crack length to failure. This model is general and can be applied to high quality welds, to welds improved by post-weld treatments or to welds containing defects. In this study, the I-P model was further modified to improve its ability to predict the fatigue resistance of welds subjected to variable loading. Each of these modifications will be discussed in turn below.

2.1 Elastic Stress Concentration Factors for the Weld Discontinuities

A stress analysis of a potential crack initiation site in welds is necessary to determine the elastic stress concentration factor (K_t) at the weld discontinuity and the stress distribution of the path along which the fatigue crack will follow. Different analysis methods have been used to determine the stress concentration factors for welded joints: work based on the plane theory of elasticity has been carried out by Turmov [7]; photoelastic solutions have been provided by Heywood and Nishida [8], and Bakski et al. [9]. Lawrence and Ho [6] have investigated the stress concentrations using the finite element method (FEM) which is very powerful for this purpose. In this study, a finite element program called ABAQUS [10] was employed to determine the notch stress concentration factors. An eight-node plane strain quadrilateral element with size less than 1/15 of the notch root radius was used.

Table 1 lists the analytical expressions for the elastic stress concentration factors (K_t) available from all sources for welds having the geometries shown in Fig. 1. A general form for K_t for weld discontinuities is:

$$K_t = \beta[1 + \alpha(t/r)^{\lambda}] \tag{2}$$

where α, β, and λ are constants determined by the weld geometry and the type of loading, t and r are the plate thickness and notch-root radius. The constants β and λ are generally 1 and 1/2 respectively so that K_t is usually $1 + \alpha(t/r)^{1/2}$.

2.2 Estimating the Fatigue Life Devoted to Crack Initiation and Growth (N_I)

The period of fatigue life devoted to crack initiation and early growth can be predicted using the local strain approach. For a weld detail subjected to combined effects of tension, induced bending and residual stress, modified Neuber's rule can be employed to simulate the local stresses and strains [6]. At the end of the first reversal (0-1) shown in Fig. 2, the local stress-strain response at the weld toe can be obtained by solving:

$$\Delta\sigma\Delta\varepsilon = (K_f^A S_1^A + K^B S_{f+1}^B \sigma_r)^2/E \qquad (3)$$

where $\Delta\sigma$, $\Delta\varepsilon$ = local stress and strain range

S_1 = remote stress

σ_r = residual stress

K_f = fatigue notch factor

A, B = indicate axial and bending loading respectively

At the end of the second reversal (1-2):

$$\Delta\sigma\Delta\varepsilon = (K_f^A \Delta S_A + K_f^B \Delta S_B)^2/E \qquad (4)$$

A difficulty in proceeding with the calculation of the local stress strain response is determining the value of K_f for the weld discontinuity. Lawrence [11] proposed the idea of a maximum value of K_f for a given weldment geometry and loading condition, K_{fmax} or the 'worst-case-notch.' K_{fmax} can be estimated using Peterson equation [12] and the value of K_t shown in Table 1:

$$K_{fmax} \cong 1 + 0.0015\alpha S_u t^{1/2} \quad (5)$$

Table 2 shows the K_{fmax} for different loading condition and weld geometry.

Using the equation for cyclic stress-strain behaviour, Eq. 6 and Eqs. 4 and 5, $\Delta\sigma$, $\Delta\varepsilon$ and mean stress σ_o can be determined.

$$\Delta\varepsilon = \frac{\Delta\sigma}{E} + 2\left(\frac{\Delta\sigma}{2K'}\right)^{1/n'} \quad (6)$$

Once the local notch stress-strain response has been estimated, the fatigue crack initiation life can be calculated using strain-life equation:

$$\frac{\Delta\varepsilon}{2} = \frac{\sigma'_f}{E}(2N_f)^b + \varepsilon'_f (2N_f)^c \quad (7)$$

The mean stress effect can be included in an expression of the following form [13]:

$$\frac{\Delta\varepsilon}{2} = \frac{\sigma'_f - \sigma_o}{E}(2N'_f)^b + \varepsilon'_f\left(\frac{\sigma'_f - \sigma_o}{\sigma_f}\right)^{c/b}(2N'_f)^c \quad (8)$$

For welds subjected to variable loading, Miner's rule is used to sum up the fatigue damage D_i of each cycle in a block of the repeated history:

$$D_{block} = \sum D_i = \sum \frac{n_i}{N_{fi}} \quad (9)$$

where n_i is the number of cycles applied at strain amplitude $\Delta\varepsilon_i/2$. Then,

crack initiation life N_I (in blocks) becomes:

$$N_I = \frac{1}{D_{block}} \tag{10}$$

A concise computer algorithm based on vector concept [14] was employed in the cycle counting.

2.3 Estimating the Fatigue Life Devoted to Crack Propagation (N_p)

Fatigue crack propagation life N_p for constant amplitude loading can be computed by integrating Paris' equation [15] from the initial crack length a_i to the final crack length a_f:

$$da/dN = C\ (\Delta K)^n \tag{11}$$

$$N_p = \int_{a_i}^{a_f} da\ /[C(\Delta K)^n] \tag{12}$$

where C and n are material constants, ΔK is the stress intensity factor range:

$$\Delta K = YS(\pi a)^{1/2} \tag{13}$$

where Y is the geometry factor.

Mean stress effect on crack propagation rate can be accounted for by substituting effective stress intensity factor range ΔK_{eff} [16] into Eq. 12. For a given shape of weld Y can be expressed conveniently by superposition of several geometry effects [17]:

$$Y = M_s M_t M_k / \phi_o \tag{14}$$

in which M_s accounts for the effect of free front surface; M_t for the finite plate width w; ϕ_o for the crack shape; M_k for nonuniform stress gradient due to the stress concentration of weld discontinuity. The analytical expression for these geometry effects are:

$$M_s = 1.12 - 0.09\ a/c \tag{15}$$

$$M_t = (\sec \pi a/2w)^{1/2} \qquad \text{for a center crack} \tag{16}$$

$$= \sin^2(\pi a/2w) + \sec^2(\pi a/2w) \qquad \text{for a single edge crack} \tag{17}$$

$$\phi_o = \int_o^{\pi/2} [1 - (1 - a^2/c^2)\ \sin^2\phi]^{1/2}\ d\phi \tag{18}$$

M_k = given in Table 3

where a is the length of minor axis of ellipse, c is the length of major axis.

When a weld is subjected to combined loading of axial, induced bending and residual stress, the total stress intensity factor range ΔK_T can be obtained by a superposition method:

$$\Delta K_T = \Delta K_A + \Delta K_B + K_r \tag{19}$$

$$K_r = F\sigma_r(\pi a)^{1/2} \tag{20}$$

where ΔK_A and ΔK_B are the stress intensity factors for tension and bending respectively, and K_r is the stress intensity factor due to residual stress and F is a function of residual stress distribution. When a crack is subjected to a distributed residual stress $\sigma_r(x)$, the stress intensity factor K_r is calculated by the integral:

$$K_r = \frac{2\sqrt{a}}{\pi} \int_0^a \frac{\sigma_r(x)}{\sqrt{a^2 - x^2}} dx \qquad (21)$$

Tada and Paris [18] derived the stress intensity factor for a crack perpendicular to the weld bead using Eq. 21. The stress intensity factor caused by the residual stresses was expressed in a simple form shown in Fig. 3. It has been shown [19] that compressive residual stress has an influence on the fatigue crack propagation behaviour in hammer-peened welds. The ability of notch compressive residual stresses to regard fatigue crack growth depends on the distribution in depth of both the residual stresses and the local stresses, and the relaxation of the residual stresses in depth [20]. Figure 4 shows the typical residual stress distribution for shot-peened specimens, and two hypothetical notch residual stress fields and their corresponding stress intensity factors [21,22]. Calculation of N_p is carried out by substituting ΔK_T into Eq. 12.

The fatigue crack propagation life N_p for a weld under variable amplitude loading can be estimated using a method developed by Socie [23] and modified by Ho [6]. The crack growth rate per block, $\Delta a/\Delta B$, is calculated by considering the crack length as being fixed at the initial crack size and summing the incremental crack extension for each cycle:

$$\Delta a/\Delta B = \sum \Delta a_i \qquad (22)$$

Combining Eqs. 11, 19, 20, Eq. 22 becomes

$$\Delta a/\Delta B = C (\pi a)^{n/2} \sum (Y_A \Delta S_A + Y_B \Delta S_B + F\sigma_r)^n \qquad (23)$$

Then, the crack propagation life N_p (in blocks) is

$$N_p = \int_{a_i}^{a_f} (\Delta B/\Delta a)\, da \tag{24}$$

3. Unanswered Questions Relating to the Use of the Total Fatigue Life Model

Most of the current fatigue tests of welds under variable loading are conducted in the intermediate life region. Welded structures are generally designed for long life use. For example, the shipbuilding industry is concerned with a fatigue design life of 20 years (about 10^8 cycles). Several investigations [24,25] have shown that for very long lives the total fatigue life model makes non-conservative estimates for both smooth and notched specimens. This discrepancy might be associated with the cycle counting method, with the damage rule used, or with the definition of initial crack length. Ho [6] has performed a limited number of welds subjected to variable loading history in the short life region. It is appropriate to question if the total fatigue life model can predict the fatigue resistance of weldments in the long-life region.

4. Scope of this Study

The total fatigue life model developed by Lawrence et al. has been further developed to predict the fatigue resistance of welds subjected to long life variable loading histories and to combined bending and torsion loading conditions.

Fatigue tests of cruciform joints and butt welds subjected to the SAE bracket history were performed. Test results were compared with

predictions made using the total fatigue life model. Post-test sectioning observations were also made to verify the validity of the total fatigue life model. The fatigue predictions made using the total fatigue life model were compared with the predictions made using alternative methods, methods based upon S-N diagrams of the actual weld details and methods based solely upon fracture mechanics.

II. WELDMENTS SUBJECTED TO VARIABLE LOADING

1. Experimental Program

1.1 Materials and Specimens

Transverse load-carrying cruciform and butt welds were studied and their geometries are shown in Fig. 1. Two kinds of cruciform joint were used. Cruciform welds with lack of penetration (LOP) were fabricated with leg length ℓ approximately equal to plate thickness of 12.7 mm (0.5 inches).

The first kind of cruciform joint was donated by General Motors' Electromotive Division and designated as MS4361. The base plate of MS4361 weldments was high strength low alloy steel. The welding electrode complied with AWS E70T-1 wire of 2 mm (5/64 in.) and was placed under a current of (40 amps at 30 volts. The welding procedure was flux-cored-arc welding process causing a final pass heat of 138 KJ/in.

A second kind of cruciform joint was donated by Caterpillar Tractor Co. and designated as 1E650. The base plate of 1E650 weldments was ASTM A370 steel. The welding procedure for 1E650 cruciform joints was semiautomatic submerged arc welding process with electrode of Lincoln L50 wire and L980 flux.

Full penetration butt welds donated by GARD INC. [25] were made by welding together two 48 inch wide, one inch thick plates of ASTM A588-A steel. Double-V-grooved butt joint design was in accordance with D1.1-80 AWS structural code. The welding process was automatic submerged arc welding process in the flat position causing an optimum heat input of 78 KJ/in. Linde WS solid wire (AWS EW) and Lincoln 882 flux were placed under 450 amps DCRP at 29 volts.

After welding, specimens were saw cut 76.2 mm (3 in.) wide for cruciform joints and 50.8 mm (2 in.). wide for butt welds from the welded panels.

1.2 Apparatus and Tests

Tests were performed in a 100 kips MTS hydraulic test system driven by a loading history generator which could store all of the loading histories and repeat these histories at different speeds. SAE bracket and transmission histories were used in this study. Figure 5 shows the histories and the peak, valley and range histograms [27]. There are 5936 reversals in one block of bracket history and 1708 reversals in one block of the transmission history.

Every specimen had four strain gages mounted at one plate thickness distance away from weld toes so that remote bending stresses could be recorded without the influence from the stress concentration of the weld. All specimens were fatigue tested to failure (separation) under load control.

1.3 Post-test Sectioning Observations

After testing, weld toe and lack of penetration site of selected welds were sectioned parallel to the loading axis through the thickness. Each specimen was sectioned eight times. The specimens were then mechanically polished and chemically milled (with a solution consisting of 85 ml of 30% H_2O_2, 15 ml of H_2O, and 5 ml of 48% HF) to remove any smearing imparted by polishing, and examined with a standard metallographic microscope. Crack lengths at the four weld toes and two lack of penetration sites were measured.

2. Predictions and Results

2.1 Predictions Made Using the Total Fatigue Life Model

Using the Initiation-Propagation model the total fatigue lives for welds subjected to variable loading have been predicted. Mechanical properties of weld metal and heat-affected-zone for GM MS4361 [6], A36 and A588-A steels [26,28] are given in Tables 4 and 5. For all cruciform welds, prediction of fatigue life was based on the mechanical properties of MS4361 HAZ and E70T-1 WM. Induced bending stresses measured from strain gages were taken into account. The residual stresses at the weld toe and root of cruciform joints were measured and are shown in Table 6. For the prediction of fatigue crack initiation life, the tensile residual stresses were taken as the yield strength of base metal. In the calculation of fatigue crack propagation life, residual stresses were not considered because their distribution and magnitude were unknown and could not be estimated. The length of LOP were measured from broken specimens. In the calculation of M_k, notch root radii were taken equal to Peterson's material constant a (K_{fmax} condition). Initial crack length of 0.25 mm (0.01 in.) was assumed for fatigue crack propagation life estimation. For cruciform joints, I-P model was applied to both the weld toe and the LOP. The fatigue initiation life calculated at the LOP was for the early crack growth and coalescence. In the calculation of fatigue crack propagation, the stress intensity factor for the LOP was obtained from Frank's result [29], see Eq. 16 and Table 3. The geometry factor in Eq. 14 is:

$$Y = M_t M_k \tag{25}$$

The stress intensity factor for crack at weld toe was based on the finite element solutions of Raju and Newman [30] for a wide range of semielliptical cracks in finite-thickness plates, see Appendix A. The influence of the local stress gradient was accounted for by multiplying these solutions by the M_k factor in Table 3. The predictions made using the total fatigue life model are given in Tables 7 through 11.

2.2 Comparisons of Predictions with Test Results

The variable amplitude loading fatigue test results are given in Tables 8, 10 and 11 and plotted in Figs. 6 through 9. The nominal stresses shown in the figures are the largest absolute value of the load history and the lives are represented as blocks. The cruciform welds were found to fail at the LOP. Butt welds failed at the toe.

Figures 10 through 11 show the correlations of the observed fatigue life and the predictions made using the total fatigue life model. Predictions agree with test results within a factor of 2 in fatigue life. In the long life region, the fatigue predictions for 1E650-B cruciform joints and ASTM A588-A steel butt welds are likely to be unconservative.

Comparison of the measured crack lengths with the predicted crack lengths are given in Tables 8 and 10. The I-P model predicted the failure sites. However, about 50% of the measured crack length at the unfailed sites were longer than the predicted crack length of < 0.25 mm (0.01 in.). The total fatigue life model utilized the low cycle fatigue properties generated from smooth specimens of HAZ with diameters of 3.8 to 4.6 mm (0.15 to 0.18 in.) in which failure is taken as 25% to 50% drop-off in load amplitude. For a 25% to 50% load drop, the fatigue crack generally

propagates through a quarter or one-half of the cross-section area, i.e., about 1 to 2 mm. If the fatigue crack initiation life is defined as the formation of an initial crack length of 1 mm (0.04 in.), the predicted crack length will be close to the observed value.

3. Predictions Made Using Other Models and Methods

There are essentially two other alternative types of prediction models reported and these are summarized in Table 12. The first type is based on the S-N diagrams for the actual weld details. The second type is based on the fracture mechanics and the fatigue crack propagation properties of smooth specimens. These prediction models will be summarized as follows.

3.1 Models Based on S-N Diagrams

The S-N diagrams approach is conventionally used in the current practice. Miner's rule is used for the cumulative damage calculations:

$$\sum \frac{n_i}{N_i} = 1 \tag{26}$$

where n_i is the number of cycles applied at stress range ΔS_i in the variable loading history and N_i is the constant amplitude fatigue life corresponding to ΔS_i. Miner's rule has been found to be unconservative in fatigue life predictions for certain types of variable loading history. Two better methods of damage accumulation have been proposed to predict the fatigue strength of weldments. The first method is using the Miner's rule but modifying the fatigue limit of the constant amplitude S-N curve for the welded detail. Figure 12 shows two typical ways of modifying the S-N

curve. One way is to extend the sloped line to the region below the fatigue limit, i.e., no cut-off. For example, Schilling and Klippstein [31] have employed an equivalent stress range of constant amplitude that produces the same fatigue damage at the variable amplitude stress range history it replaces. As the negative reciprocal slope of S-N curve is about three for structural steel and structural details, Schilling et al. suggested the use of the 'root-mean-cube (RMC) stress range' for welded bridge details subjected to variable amplitude loading history. The other way suggested in BS 5400 [32] is bending the S-N curve from a slope of -1/m to -1/(m+2) at 10^7 cycles. The second method for improving damage accumulation is to introduce a nonlinear damage rule. In the Joehnk and Zwerneman's nonlinear damage model [3], the ratio of damage to stress range will increase in a nonlinear form as the stress range decreases. Effective stress ranges were defined for subcycles first, then Miner's rule was employed to calculate the damage of subcycles.

Two fatigue prediction models have been proposed to predict the fatigue resistance of welds subjected to variable loading history using constant amplitude S-N diagram and will be discussed below: one uses Miner's rule and an extended S-N curve - the Munse's fatigue criterion and the other uses an empirical relationship based on test results - Gurney's model.

Munse's Fatigue Design Criterion

Three factors have been considered in Munse's fatigue design criterion [1]. These are: (a) the mean fatigue resistance of the weld details, (b) a 'random load factor' (ξ) that is a function of variable amplitude loading

history and slope of the mean S-N curve, and (c) a 'reliability factor' (R_F) (roughly the inverse of the safety factor) that is a function of the slope of the mean S-N curve, level of reliability, and a coefficient of variation.

The maximum allowable fatigue stress range ΔS_D for welds subjected to variable loading history is obtained from the following equation:

$$\Delta S_D = \Delta S_N \cdot \xi \cdot R_F \tag{27}$$

where ΔS_N is the constant amplitude stress range at fatigue life of N cycles. For welds subjected to a constant amplitude fatigue stress-range (ΔS_N), the mean fatigue life N is given by the relationship:

$$N = \frac{C}{(\Delta S_N)^m} \tag{28}$$

where C and m are empirical constants obtained from a least-squares analysis of S-N diagram data. Munse's criterion uses the extended straight S-N line at ration R=0 as its basis (see Fig. 12) and neglects the effect of mean stress, material properties and residual stress.

After cycle counting, the variable load history is plotted in a stress range histogram. Mean stress level and sequence effect are regarded as secondary effects. Since random loadings for weld details usually cannot be determined exactly, Munse's criterion uses probability distribution functions to represent the weld fatigue loading. Six probability distribution functions are employed to represent different common variable loading histories: beta, lognormal, Weibull, exponential, Rayleigh and a

shifted exponential distribution function. It is necessary to determine which distribution or distributions provides the best fit to a given loading history. The random load factor in Munse's fatigue criterion are for a desired life of 10^8 cycles. In this study, the values of random load factor have been derived for any arbitrary fatigue life and are shown in Table 13.

The reliability factor is given by:

$$R_F = \left\{\frac{[P_F(N)]\Omega_N^{1.08}}{\Gamma(1 + \Omega_N^{1.08})}\right\}^{1/m} \tag{29}$$

where $P_F(N)$ is the probability of failure, Ω_N is the total uncertainty for fatigue life of N cycles and Γ is the gamma function. Mean values of reliability factor for various levels of reliability were also provided (see Fig. 13).

Gurney's Model

Gurney [2] performed fatigue tests on fillet welded joints using simple variable loading history. It was found that the logarithm of number of blocks to failure varied linearly with the ratio of the subcycle's stress range to the maximum stress range in the history:

$$N_b = N_c \left\{\left[\prod_2^n \frac{N_i - 1}{N_i}\right]^{p_i}\right\} \tag{30}$$

where N_b = the fatigue life in blocks

N_c = the fatigue life in cycles at maximum stress range in the block history

N_i = number of cycles per block equal or exceeding p_i times the maximum stress range in the block history

n = total number of cycles in a block

The parameter contained within the braces is the random load factor.

3.2 Methods Based upon Fracture Mechanics

Methods based upon fracture mechanics ignore the fatigue crack initiation phase and calculate the fatigue crack propagation life only. Maddox [4] used linear fracture mechanics and Miner's rule to predict the fatigue life of welds subjected to variable loading history. Miner's rule was found to be accurate for welds under loading histories without stress interaction.

Barsom [5] used a single stress intensity factor parameter, root-mean-square stress intensity factor, to define the crack growth rate under both constant and variable amplitude loadings. The root-mean-square stress intensity factor, ΔK_{rms}, is characteristic of the load distribution and is independent of the order of the cyclic load fluctuations. Hudson [33] applied the root-mean-square (RMS) method for random loading history with variable minimum load. This simple RMS approach has been shown applicable for loading history with random sequences. The root mean square stresses are defined as:

$$S_{max}^{rms} = \left[\frac{1}{N}\sum_{n=1}^{N}(S_{max}^{n})^2\right]^{1/2} \tag{31}$$

and

$$S_{min}^{rms} = [\frac{1}{N}\sum_{n=1}^{N}(S_{min}^{n})^2]^{1/2} \quad (32)$$

where S_{max} and S_{min} are the maximum and minimum stresses for each cycle respectively and N is the total number of cycles for the random loading history.

The root-mean-square stress intensity factor range is calculated from

$$\Delta K_{rms} = K_{max}^{rms} - K_{min}^{rms} \quad (33)$$

Calculation of fatigue crack propagation life is through the substitution of Eqn. 33 into fatigue propagation model.

3.3 Comparisons of Predictions with Test Results

Fatigue predictions have been made using the Miner's rule (based on the extended S-N curve), Munse's fatigue criterion, Gurney's model and the RMS method. Figures 14 and 15 show the constant amplitude S-N curves obtained from previous studies [6,26,34]. Table 14 shows the values of C and m obtained from the S-N diagram with stress ratio R=0. The characteristic parameters for the SAE bracket and transmission history are given in Table 15. Rainflow method was applied to cycle-counting the variable loading history. The predictions made using these models are given in Tables 16 and 17.

The reliability factor of Munse's fatigue criterion was neglected to predict the mean fatigue life. The agreement between the predictions and test results is good for welds subjected to bracket history. The predictions made for welds under transmission history are unconservative. Fatigue life predictions made using Miner's rule (based on extended S-N curve) and Munse's fatigue criterion are similar for the SAE loading history in this study.

Gurney's model gave conservative predictions for welds subjected to the SAE bracket and transmission history in this study.

For welds subjected to axial loading combined with bending the calculation of stress intensity factor using RMS methods is not as simple as that for pure axial loading. Since bending has minor effect on the fatigue resistance of internal crack [6] the RMS methods was applied to predict the fatigue life of cruciform joints failed at LOP. In this study, the fatigue crack propagation life estimated from RMS method were the same as the fatigue crack propagation life estimated by the I-P model. RMS method gave conservative predictions for welds in this study.

4. Summary

The predictions made using the total fatigue life model consistently agreed with the test results within a factor of three. Mean fatigue life predictions made using Munse's fatigue criterion and Miner's rule were close to the test results for welds subjected to little mean stress biased history, such as SAE bracket history, but appeared unconservative for welds subjected to SAE transmission history which has a strong tensile-biased mean stress. Gurney's model and RMS method were conservative in this

study. The comparisons of the predicted life with test results are given in Figs. 16 through 20.

Table 1

Stress Concentration Factor K_t for Weldments

Type of Weld	Reference	Discontinuity	Loading	K_t^*	Analysis Method
butt weld	G1**, [6]	toe	axial	$\alpha = 0.27(\tan\theta)^{0.25}$ $\beta = 1,\ \lambda = 0.5$	FEM
	G1, [6]	toe	bending	$\alpha = 0.165(\tan\theta)^{0.167}$ $\beta = 1,\ \lambda = 0.5$	FEM
	G1, [7]	toe	axial	$\alpha = 1.1h^{1.5}[(w/t)^2+1]/t^{1.5}$ $\beta = 1,\ \lambda = 0.5$	elasticity
	G2, [8]	toe	axial	$\alpha = \{1-\exp[0.90\theta\pi/180\Delta^{0.5}]\}/\{1-\exp[-0.45\pi\Delta^{0.5}]\}x[1-0.48\exp(-0.74w/t)]x\{h/[2.8(2h+t)-2t]\}^{\lambda}$ $\Delta = (2h+t)/(2h)^{\lambda}$ $\beta = 1$ $\lambda = 0.65-0.1\exp(-0.63w/t)$	photoelasticity
cruciform joint of fillet welds	G3, [6]	toe	axial	$\alpha = 0.35(\tan\theta)^{0.25}[1+1.1(c/\ell)^{1.65}]$ $\beta = 1,\ \lambda = 0.5$	FEM
	G3, [6]	toe	bending	$\alpha = 0.21(\tan\theta)^{0.167}$ $\beta = 1,\ \lambda = 0.5$	FEM

* $K_t = \beta[1+\alpha(t/r)^{\lambda}]$

** geometry in Fig. 1

Table 1 Continued

Type of Weld	Reference	Discontinuity	Loading	K_t	Analysis Method
	G3, [6]	LOP	axial	$\alpha = 1.15(\tan\theta)^{-0.25}(c/\ell)^{0.5}$ $\beta = 1,\ \lambda = 0.5$	FEM
	G3, [6]	LOP	bending	$\alpha = 3.22(c/t)^{0.12}$ $\beta = 1,\ \lambda = 0.5$	FEM
	G4, [7]	toe	axial	$\alpha = 0.2(2-\ell/t)^{0.5}$ $\beta = 1,\ \lambda = 0.5$ (for $\ell_1 = \ell_2$)	elasticity
	G4, [7]	toe	axial	$\alpha = 0.2(2-\ell_1/\ell_2)^{0.5}$ $\beta = 1,\ \lambda = 0.5$	elasticity
	G5, [7]	toe	axial	$\alpha = 0.4(2-\ell/t)^{0.5}$ $\beta = 1,\ \lambda = 0.5$ (for $\ell_1 = \ell_2$)	elasticity
tee joint of fillet weld	G6, [8]	toe	axial	$\alpha = \{1-\exp[-0.9\theta\pi/180\Delta^{0.5}]\}/\{1-\exp[-0.45\pi\Delta^{0.5}]\}x\{h/[2.8(2h+t)-2t]\}^{\lambda}$ $\Delta = (2h+t)/(2h)$ $\beta = 1,\ \lambda = 0.65$	photoelasticity
	G7, [9]	toe	axial	$\alpha = [(\mu-1)/(\mu^2+1.6)]^{0.5}\sin\theta$ $\beta = 1+3.7[\gamma\sin(\theta-15^0)]^2$ $\lambda = 0.5$ $\mu = (2\ell_2+t)/t$ $\gamma = 2c/t$	photoelasticity

Table 1 Continued

Type of Weld	Reference	Discontinuity	Loading	K_t	Analysis Method
	G7, [9]	toe	bending	$\alpha = 0.3(\mu-1)^{0.2}\sin\theta$ $\beta = 1+2.3[\gamma\sin(\theta-15^0)]^2$ $\lambda = 0.5$ $\mu = (2\ell_2+t)/t$ $\gamma = 2c/t$	photoelasticity
	G8, [6]	toe	axial	$\alpha = 0.35+0.1(2c/t)^{1.78}$ $\beta = 1,\ \lambda = 0.5$	FEM
	G8, [6]	toe	bending	$\alpha = 0.19$ $\beta = 1,\ \lambda = 0.5$	FEM
double lap joint of fillet weld	G9, [6]	toe	axial	$\alpha = 0.6(\tan\theta)^{0.25}(t/\ell_1)^{0.5}$ $\beta = 1,\ \lambda = 0.5$	FEM
	G9, [6]	toe	bending	$\alpha = 0.24(\tan\theta)^{0.167}$ $\beta = 1,\ \lambda = 0.5$	FEM
	G9, [6]	root	axial	$\alpha = 0.5(\ell_1/\ell_2)^{0.12}$ $\beta = 1,\ \lambda = 0.5$	FEM
	G9, [9]	toe	axial	$\alpha = [(\mu-1)/\mu^2+1.6)]^{0.5}\sin\theta$ $\beta = 1+3.7[\eta\sin(\theta-15^0)]^2$ $\lambda = 0.5$ $\eta = (t-2h)/t$	photoelasticity
	G9, [9]	toe	bending	$\alpha = 0.3(\mu-1)^{0.2}\sin\theta$ $\beta = 1+2.3[\eta\sin(\theta-15^0)]^2$ $\lambda = 0.5$	photoelasticity

Table 1 Continued

Type of Weld	Reference	Discontinuity	Loading	K_t	Analysis Method
as-rolled surface weld with reinforcement removed	G10, [6]	-	axial	$\alpha = 2, \beta = 1, \lambda = 0.5$ $t = d$ = surface roughness	-
			bending	$\alpha = 1.8, \beta = 1, \lambda = 0.5$ $t = d$ = surface roughness	-
weld with undercut	G11, [37]	toe	axial	$\alpha = 2, \lambda = 0.5, t = d$ = undercut $\beta = K_{t_0} = \beta_0[1+\alpha_0(t/r_0)^{\lambda_0}]$	-
			bending	$\alpha = 1.8, \lambda = 0.5, t = d$ = undercut $\beta = K_{t_0} = \beta_0[1+\alpha_0(t/r_0)^{\lambda_0}]$	-

Table 2

K_{fmax} for Steel Weldments

Type of Weld	Reference	Discontinuity	Loading	r_c & K_{fmax}
butt weld	G1*, [6,7]	toe	axial, bending	$r_c = a$ $K_{fmax} = 1+0.0015\alpha S_u t^{0.5}$
	G2, [8]	toe	axial	$r_c = [(1-\lambda)/\lambda]a$ $K_{fmax} = 1+(1-\lambda)[9.1 \times 10^{-5}\lambda/(1-\lambda)]^{\lambda}\alpha S_u{}^{2\lambda} t^{\lambda}$
cruciform joint	G3, G4, G5 [6,7]	toe, LOP	axial, bending	$r_c = a$ $K_{fmax} = 1+0.0015\alpha S_u t^{0.5}$
tee joint of fillet weld	G6, [8]	toe	axial	$r_c = 0.54a$ $K_{fmax} = 1+2.8 \times 10^{-4}\alpha S_u{}^{1.3} t^{0.65}$
	G7, [6]	toe	axial, bending	$r_c = \{\{a(\beta-1)+[a^2(\beta-1)^2+ta\alpha^2\beta^2]^{0.5}\}/t^{0.5}\alpha\beta\}^2$ K_{fmax} can be obtained by substituting r_c into Peterson's K_f equation
	G8, [6]	toe, LOP	axial, bending	$r_c = a$ $K_{fmax} = 1+0.0015\alpha S_u t^{0.5}$
double lap joint of fillet weld	G9, [6]	toe	axial, bending	$r_c = a$ $K_{fmax} = 1+0.0015\alpha S_u t^{0.5}$
	G9, [9]	toe	axial, bending	$r_c = \{\{a(\beta-1)+[a^2(\beta-1)^2+ta\alpha^2\beta^2]^{0.5}\}/t^{0.5}\alpha\beta\}^2$ K_{fmax} can be obtained by substituting r_c into Peterson's K_f equation

SI units = r_c & t (mm), S_u (MPa)

*: geometry in Fig. 1

Table 2 Continued

Type of Weld	Reference	Discontinuity	Loading	r_c & K_{fmax}
as-rolled surface weld with reinforcement removed	G10, [6]	-	axial, bending	$r_c = a$ $K_{fmax} = 1+0.0015\alpha S_u t^{0.5}$
weld with undercut	G11, [37]	toe	axial, bending	$r_c = \{\{a(\beta-1)+(a^2(\beta-1)^2+ta\alpha^2\beta^2]^{0.5}\}/t^{0.5}\alpha\beta\}^2$ K_{fmax} can be obtained by substituting r_c into Peterson's K_f equation

Table 3

The Geometry Factor M_k for Weldments

Welds	Site	Loading	M_k	Reference
transverse load-carrying fillet welds	toe	axial	$M_k = 1+(K_t-1)\exp[-22(K_t-1)^{0.85} a/t]$	[6]
		bending	$M_k = 1+(K_t-1)\exp[-42(K_t-1)^{0.65} a/t]$	[6]
	LOP	axial	$M_k = [A_1+A_2(a/w)]$ $A_1 = 0.528+3.287(\ell/t)-4.361(\ell/t)^2 +3.696(\ell/t)^3-1.874(\ell/t)^4+ 0.415(\ell/t)^5$ $A_2 = 0.218+2.717(\ell/t)-10.171(\ell/t)^2 13.122(\ell/t)^3-7.755(\ell/t)^4+ 1.785(\ell/t)^5$	[29]
transverse non-load-carrying fillet welds	toe	axial	$M_k = (0.8857)^k(0.848)^{1-k}(\ell/2t)^{0.063k} a/t)^{-q}$ for $0.1 \le a/t \le 0.65$ $k = 1.0 - \log \Lambda/\log 4.49$ $q = 0.054\Lambda + 0.2255$ where Λ is the ratio between the thickness of the attachment plate and main plate.	[35]
transverse butt welds	toe	axial	$M_k = (5a/t)^{-q}$ $q = 1/2.3 \log(1+0.0588\theta)$	[35]

Table 4

Mechanical Properties of GM MS4361 HAZ and E70T-1 WM

Monotonic Properties		MS4361 HAZ	1E70T-1 WM
Elastic Modulus, GPa (ksi)	E	198 (28700)	220 (30740)
Yield Strength (0.2%), MPa (ksi)	S_y	414 (60)	462 (67)
Tensile Strength, MPa (ksi)	UTS	628 (91)	758 (110)
Reduction in Area	%RS	61%	48%
True Fracture Strength, MPa (ksi)	σ_f	917 (133)	1462 (212)
True Fracture Ductility	ε_f	0.75	0.93
Strength Coefficient	K	-	-
Strain Hardening Exponent	n	-	-
Cyclic Properties			
Fatigue Ductility Coefficient	ε'_f	0.28	0.37
Fatigue Ductility Exponent	c	-0.52	-0.55
Fatigue Strength Coefficient, MPa (ksi)	σ'_f	828 (120)	1076 (156)
Fatigue Strength Exponent	b	-0.082	-0.083
Cyclic Strength Coefficient, MPa (ksi)	K'	1020 (148)	1379 (200)
Cyclic Strain Hardening Exponent	n'	0.18	0.17
Cyclic Yield Strength, MPa (ksi)	S'_y	345 (50)	490 (71)
Propagation Properties			
Crack Growth Coefficient (R=0)	C	1.86×10^{-12}	5.27×10^{-11}
Crack Growth Exponent (R=0)	n	3.3	2.4
Fracture Toughness, $MPa\sqrt{m}$ (R=0)	K_c	77	110

Table 5

Mechanical Properties of ASTM A36 HAZ and A588-A HAZ

Monotonic Properties		A36 HAZ	A588-A HAZ
Elastic Modulus, GPa (ksi)	E	210 (30400)	203 (29400)
Yield Strength (0.2%), MPa (ksi)	S_y	565 (82)	731 (106)
Tensile Strength, MPa (ksi)	UTS	752 (109)	848 (123)
Reduction in Area	%RS	49%	63%
True Fracture Strength, MPa (ksi)	σ_f	1007 (146)	1352 (196)
True Fracture Ductility	ε_f	0.78	1.00
Strength Coefficient	K	1103 (106)	1579 (229)
Strain Hardening Exponent	n	0.11	0.12
Cyclic Properties			
Fatigue Ductility Coefficient	ε'_f	0.28	0.37
Fatigue Ductility Exponent	c	-0.60	-0.60
Fatigue Strength Coefficient, MPa (ksi)	σ'_f	1090 (158)	1200 (174)
Fatigue Strength Exponent	b	-0.091	-0.084
Cyclic Strength Coefficient, MPa (ksi)	K'	1110 (161)	1117 (162)
Cyclic Strain Hardening Exponent	n'	0.15	0.14
Cyclic Yield Strength, MPa (ksi)	S'_y	434 (63)	496 (72)
Propagation Properties			
Crack Growth Coefficient (R=0)	C	6.89×10^{-12}	6.89×10^{-12}
Crack Growth Exponent (R=0)	n	3.0	3.0
Fracture Toughness, $MPa\sqrt{m}$ (R=0)	K_c	85	88

Table 6

Longitudinal Residual Stress Measurements for 1E650-B Cruciform Joints

Site	Longitudinal Residual Stress, MPa			
toe	160 ± 66	-31 ± 32	-162 ± 21	26 ± 26
	48 ± 43	-88 ± 37	126 ± 39	4 ± 34
	30 ± 36	-104 ± 44	46 ± 39	98 ± 46
LOP	251 ± 32	-35 ± 33	8 ± 23	205 ± 20
	-50 ± 21	-180 ± 32	195 ± 72	28 ± 48
	101 ± 21	104 ± 25	-396 ± 61	190 ± 61

Table 7

Geometry of MS4361 Cruciform Welds at Notch Sites

Specimen No.	Site	ℓ_1 mm.	ℓ_2 mm.	LOP c mm.	K^A_{fmax}	K^B_{fmax}
3-2	LOP1	10.2	10.2	3.8	4.68	0.49
	toe1	10.2	10.2	3.8	2.64	1.80
	toe2	12.7	9.7	3.8	2.46	1.75
	LOP2	10.7	8.9	2.0	4.25	0.31
	toe3	10.7	8.9	2.0	2.42	1.78
	toe4	11.4	10.2	2.0	2.40	1.78
3-1	LOP1	10.2	10.2	3.8	4.68	0.49
	toe1	10.2	10.2	3.8	2.64	1.80
	toe2	10.7	10.7	3.8	2.60	1.79
	LOP2	10.7	8.9	2.0	4.25	0.31
	toe3	10.7	8.9	2.0	2.42	1.78
	toe4	11.4	11.4	2.0	2.40	1.78
3-3	LOP1	10.2	9.7	3.8	4.85	0.54
	toe1	10.2	9.7	3.8	2.63	1.79
	toe2	12.2	9.7	3.8	2.49	1.76
	LOP2	11.4	9.7	2.0	4.08	0.26
	toe3	11.4	9.7	2.0	2.39	1.74
	toe4	12.7	12.7	2.0	2.36	1.76
7-5	LOP1	12.7	12.7	3.8	4.22	0.30
	toe1	12.7	12.7	3.8	2.48	1.76
	toe2	15.2	12.7	3.8	2.37	1.73
	LOP2	12.7	12.7	3.6	4.13	0.27
	toe3	12.7	12.7	3.6	2.46	1.76
	toe4	12.7	12.7	3.6	2.46	1.76
2-4	LOP1	10.2	10.2	3.8	4.68	0.49
	toe1	10.2	10.2	3.8	2.64	1.80
	toe2	12.7	11.9	3.8	2.48	1.76
	LOP2	12.7	12.7	3.8	4.22	0.30
	toe3	12.7	12.7	3.8	2.48	1.76
	toe4	13.2	11.4	3.8	2.45	1.75
5-4	LOP1	12.7	12.7	3.8	4.22	0.30
	toe1	12.7	12.7	3.8	2.48	1.76
	toe2	15.2	12.7	3.8	2.37	1.73
	LOP2	12.7	12.7	3.6	4.13	0.27
	toe3	12.7	12.7	3.6	2.46	1.76
	toe4	12.7	12.7	3.6	2.46	1.76

Table 8

Fatigue Life Predictions and Test Results for MS4361 Cruciform Welds Under SAE Bracket History

Spec. No.	Site	S^A_{min} MPa	S^B_o MPa	Bending Factor	Actual Life, blocks	c mm. Exp.	c mm. Pred.	Life Predicted, N_T blocks
3-2	LOP1	-209	107	0.20	491	failed		434
	toe1	-209	107	0.20	-	0.90	0.53	1000
	toe2	-209	-107	-0.20	-	0.32	< 0.25	49080
	LOP2	-209	109	0.10	-	0.10	2.00	693
	toe3	-209	109	0.10	-	0.	< 0.25	1490
	toe4	-209	-109	-0.10	-	0.	< 0.25	31020
3-1	LOP1	-184	52	0.20	575	failed		658
	toe1	-184	52	0.20	-	1.10	< 0.25	1900
	toe2	-184	-52	-0.20	-	0.05	< 0.25	17570
	LOP2	-184	64	0.10	-	0.67	1.27	1080
	toe3	-184	64	0.10	-	0.18	< 0.25	3120
	toe4	-184	-64	-0.10	-	0.	< 0.25	69780
3-3	LOP1	-147	91	0.14	1450	failed		1350
	toe1	-147	91	0.14	-	0.	< 0.25	6030
	toe2	-147	-91	-0.14	-	0.	< 0.25	839040
	LOP2	-147	76	0.07	-	0.18	< 0.25	3480
	toe3	-147	76	0.07	-	0.	< 0.25	12910
	toe4	-147	-76	-0.07	-	0.	< 0.25	751660
7-5	LOP1	-152	62	0.20	1825	failed		2290
	toe1	-152	62	0.20	-	failed	< 0.25	5500
	toe2	-152	-62	-0.20	-	0.	< 0.25	1180000
	LOP2	-152	44	0.08	-	0.20	7.60	2580
	toe3	-152	44	0.08	-	0.	< 0.25	10030
	toe4	-152	-44	-0.08	-	0.	< 0.25	50400
2-4	LOP1	-139	69	0.16	2933	failed		2080
	toe1	-139	69	0.16	-	0.	< 0.25	8380
	toe2	-139	-69	-0.16	-	0.	< 0.25	1477770
	LOP2	-139	54	0.09	-	0.70	< 0.25	3850
	toe3	-139	54	0.09	-	0.24	< 0.25	16000
	toe4	-139	-54	-0.09	-	0.	< 0.25	141700
5-4	LOP1	-148	33	0.21	3851	failed		2630
	toe1	-148	33	0.21	-	failed	< 0.25	7080
	toe2	-148	-33	-0.21	-	0.	< 0.25	159010
	LOP2	-148	33	0.11	-	1.02	7.60	3010
	toe3	-148	33	0.11	-	0.	< 0.25	11300
	toe4	-148	-33	-0.11	-	0.	< 0.25	55830

Table 9

Geometry of 1E650-B Cruciform Welds at Notch Sites

Specimen No.	Site	ℓ_1 mm.	ℓ_2 mm.	LOP c mm.	K^A_{fmax}	K^B_{fmax}
B-19	LOP1	8.9	8.9	5.1	5.48	0.93
	toe1	8.9	8.9	5.1	2.97	1.82
	toe2	9.7	9.2	5.1	2.86	1.80
	LOP2	9.2	9.2	4.6	5.22	0.77
	toe3	9.2	9.2	4.6	2.85	1.81
	toe4	9.7	9.2	4.6	2.78	1.80
B-23	LOP1	8.9	8.9	4.6	5.29	0.81
	toe1	8.9	8.9	4.6	2.88	1.82
	toe2	9.7	9.2	4.6	2.78	1.80
	LOP2	9.2	9.2	4.1	5.02	0.66
	toe3	9.2	9.2	4.1	2.76	1.81
	toe4	9.7	9.2	4.1	2.71	1.80
B-14	LOP1	8.9	8.9	5.1	5.48	0.93
	toe1	8.9	8.9	5.1	2.97	1.82
	toe2	9.7	9.2	5.1	2.86	1.80
	LOP2	8.9	8.9	4.1	5.09	0.71
	toe3	8.9	8.9	4.1	2.79	1.82
	toe4	9.7	8.9	4.1	2.71	1.80
B-21	LOP1	8.9	8.9	5.1	5.48	0.93
	toe1	8.9	8.9	5.1	2.97	1.82
	toe2	9.4	8.9	5.1	2.90	1.81
	LOP2	8.9	8.9	5.1	5.48	0.93
	toe3	8.9	8.9	5.1	2.97	1.82
	toe4	9.7	9.2	5.1	2.86	1.80
B-10	LOP1	8.9	8.9	5.1	5.48	0.93
	toe1	8.9	8.9	5.1	2.97	1.82
	toe2	9.4	8.6	5.1	2.89	1.80
	LOP2	9.2	9.2	5.1	5.40	0.87
	toe3	9.2	9.2	5.1	2.94	1.81
	toe4	9.4	9.4	5.1	2.94	1.81

Table 9 (Continued)

Specimen No.	Site	ℓ_1 mm.	ℓ_2 mm.	LOP c mm.	K^A_{fmax}	K^B_{fmax}
B-1	LOP1	9.2	9.2	5.6	5.57	0.98
	toe1	9.2	9.2	5.6	3.03	1.81
	toe2	9.4	9.4	5.6	3.03	1.81
	LOP2	8.9	8.9	4.3	5.19	0.76
	toe3	8.9	8.9	4.3	2.84	1.82
	toe4	9.4	8.6	4.3	2.77	1.80
B-18	LOP1	8.9	8.9	5.1	5.48	0.93
	toe1	8.9	8.9	5.1	2.97	1.82
	toe2	9.7	9.2	5.1	2.86	1.80
	LOP2	9.2	9.2	4.6	5.22	0.77
	toe3	9.2	9.2	4.6	2.85	1.81
	toe4	9.7	9.2	4.6	2.78	1.80

Table 10

Fatigue Life Predictions and Test Results for 1E650-B Cruciform Welds Under SAE Bracket History

Spec. No.	Site	S^A_{min} MPa	S^B_o MPa	Bending Factor	Actual Life, blocks	c mm. Exp.	c mm. Pred.	Life Predicted, N_T blocks
B-19	LOP1	-207	34	0.20	297	failed		230
	toe1	-207	34	0.20	-	0.80	0.30	1050
	toe2	-207	-34	-0.20	-	0.	< 0.25	2250
	LOP2	-207	17	0.10	-	2.40	3.81	287
	toe3	-207	17	0.10	-	0.	< 0.25	1460
	toe4	-207	-17	-0.10	-	0.	< 0.25	3150
B-23	LOP1	-193	34	0.20	547	failed		335
	toe1	-193	34	0.20	-	0.	< 0.25	1398
	toe2	-193	-34	-0.20	-	0.	< 0.25	7610
	LOP2	-193	17	0.10	-	4.20	4.32	419
	toe3	-193	17	0.10	-	0.12	< 0.25	2030
	toe4	-193	-17	-0.10	-	0.	< 0.25	4780
B-14	LOP1	-108	17	0.15	1212	failed		3270
	toe1	-108	17	0.15	-	0.	< 0.25	32100
	toe2	-108	-17	-0.15	-	0.	< 0.25	244400
	LOP2	-108	11	0.04	-	1.00	< 0.25	5420
	toe3	-108	11	0.04	-	0.	< 0.25	81500
	toe4	-108	-11	-0.04	-	0.	< 0.25	196000
B-21	LOP1	-122	74	0.11	1220	failed		1600
	toe1	-122	74	0.11	-	0.60	< 0.25	128900
	toe2	-122	-74	-0.11	-	0.	< 0.25	738000
	LOP2	-122	40	0.06	-	1.20	< 0.25	1608
	toe3	-122	40	0.06	-	0.	< 0.25	17900
	toe4	-122	-40	-0.06	-	0.	< 0.25	66100
B-10	LOP1	-114	21	0.18	1270	failed		2320
	toe1	-114	21	0.18	-	0.	< 0.25	19400
	toe2	-114	-21	-0.18	-	0.	< 0.25	174000
	LOP2	-114	21	0.04	-	3.50	< 0.25	2570
	toe3	-114	21	0.04	-	0.	< 0.25	37900
	toe4	-114	-21	-0.04	-	0.	< 0.25	67400

Table 10 (Continued)

Spec. No.	Site	S^A_{min} MPa	S^B_o MPa	Bending Factor	Annual Life, blocks	c mm. Exp.	c mm. Pred.	Life Predicted, N_T blocks
B-1	LOP1	-100	54	0.08	1536	failed		3880
	toe1	-100	54	0.08	-	6.70	7.62	50000
	toe2	-100	-54	-0.08	-	0.	< 0.25	362800
	LOP2	-100	34	0.02	-	2.01	< 0.25	7650
	toe3	-100	34	0.02	-	0.	< 0.25	115000
	toe4	-100	-34	-0.02	-	0.	< 0.25	351000
B-18	LOP1	-83	38	0.20	3004	failed		16600
	toe1	-83	38	0.20	-	1.52	< 0.25	393000
	toe2	-83	-38	-0.20	-	0.	< 0.25	2647800
	LOP2	-83	6	0.10	-	0.05	< 0.25	30970
	toe3	-83	6	0.10	-	0.	< 0.25	666700
	toe4	-83	-6	-0.10	-	0.	< 0.25	2979000

Table 11

Fatigue Predictions and Test Results for ASTM A588-A Butt Welds under SAE Bracket History and ASTM A36 Butt Welds under SAE Transmission History

Spec. No.	Flank Angle θ, deg.	K^A_{fmax}	K^B_{fmax}	S^A MPa	S^B_o MPa	Bending Factor	Actual Life, blocks	Life Predicted, N_T blocks
A588-A				(min.)				
3	68.0	4.62	2.43	-212	8	0.19	334	333
5	68.0	4.62	2.43	-164	17	0.20	801	727
6	68.0	4.62	2.43	-148	81	0.10	961	2370
7	68.0	4.62	2.43	-142	74	0.10	1192	2781
A36				(max.)				
25-2	50.6	3.50	-	344	-	-	229	257
15-5	50.6	3.50	-	344	-	-	228	257
25-5	50.6	3.50	-	337	-	-	240	275
16-5	50.6	3.50	-	335	-	-	306	281
15-2	50.6	3.50	-	282	-	-	529	520
43-4	50.6	3.50	-	282	-	-	615	520
16-6	50.6	3.50	-	282	-	-	677	520
16-3	50.6	3.50	-	282	-	-	655	520
25-3	50.6	3.50	-	282	-	-	720	520
15-1	50.6	3.50	-	229	-	-	1351	1180
43-6	50.6	3.50	-	229	-	-	1188	1180
15-6	50.6	3.50	-	229	-	-	1999	1180

Table 12

Summary of Fatigue Life Prediction Models for Weldments Subjected to Variable Loading

	Basis	Proposed by	Model
1.	the total fatigue life model	Lawrence Ho	$N_T = N_I + N_P$ N_T : total fatigue life N_I : fatigue crack initiation life N_P : fatigue crack propagation life
2.	S-N diagram	Miner	$\sum (n_i/N_i) = 1$ n_i : no. of cycles applied at ΔS_i N_i : no. of cycles to failure at ΔS_i linear damage accumulation
		Zwerneman Joehnk	$\Delta S_{eff} = \Delta S_i (\Delta S_{max}/\Delta S_i)^a$ ΔS_{eff} : effective stress range at ΔS_i ΔS_{max} : maximum stress range a : vary with loading history nonlinear cumulative damage
		Gurney	$N_b = N_c [\pi_2^n (N_{i-1}/N_i)^{p_i}]$ N_b : no. of blocks to failure N_c : no. of cycles to failure at ΔS_{max} N_i : no. of cycles per block equal to or exceeding p_i times the maximum stress in one block
		Munse	$\Delta S_D = \Delta S_N * \xi * R_F$ ΔS_D : allowable maximum stress range ΔS_N : maximum stress range in life N ξ : probabilistic random load factor R_F : reliability factor
3.	fracture mechanics	Barsom	$\Delta K_{rms} = [(\sum \Delta K_i)^2/n]^{1/2}$ ΔK_{rms} : root mean square stress intensity factor range fatigue crack propagation life only

Table 13

Random Load Factors for Distribution Functions

Distribution Function	Random Load Factor, ξ
beta	$\{[\Gamma(q)\Gamma(m+q+r)]/[\Gamma(m+q)\Gamma(q+r)]\}^{1/m}$
Weibull	$(\ln N)^{1/k}[\Gamma(1+m/k)]^{-1/m}$
exponential	$(\ln N)[\Gamma(1+m)]^{-1/m}$
Rayleigh	$(\ln N)^{1/2}[\Gamma(1+m/2)]^{-1/m}$
lognormal	$(1+\delta_s^2)^{-m/2}\exp\{\gamma[\ln(1+\delta_s^2)]^{1/2}\}$ $\delta_s = \sigma_s/\mu_s$ $\gamma = \Phi^{-1}(1-N^{-1})$
shifted exponential	$[\sum_{n=0}^{m} m!/(m-n)!(\ln N)^{-n}(1-\alpha)^n\alpha^{m-n}]^{-1/m}$ $\alpha = a/[a+\mu_s(\ln N_b)]$

Table 14

Constant Amplitude Fatigue Test Results (R = 0)

Welds	S-N Diagram	
	Slope, m	$\log_{10} C$
fillet welds:		
GM MS 4361	4.35	11.71
CT 1E650-B	3.48	11.06
butt welds:		
ASTM A588-A	4.23	11.33
ASTM A36	3.95	11.33

Table 15

Characteristic Parameters for SAE Bracket and Transmission History

Characteristic Parameter	Bracket History	Transmission History
beta distribution		
q	2.781	2.066
r	6.696	6.781
Weibull distribution		
k	2.18	1.78
mean ΔS (μ_s)	0.294 ΔS_{max}	0.234 ΔS_{max}
standard deviation of ΔS, (σ_s)	0.141 ΔS_{max}	0.135 ΔS_{max}
S_{max}^{rms}	0.254 $\lvert S_{min} \rvert$	0.593 $\lvert S_{max} \rvert$
S_{min}^{rms}	-0.351 $\lvert S_{min} \rvert$	-0.222 $\lvert S_{max} \rvert$
Gurney's random load factor	7.755×10^{-3}	2.247×10^{-2}

Table 16

Mean Fatigue Life Predictions for 1E650-B and GM4361 Cruciform Joints of Fillet Weld under SAE Bracket History

Spec. No.	Life Predicted, blocks							
	Miner's Rule	Gurney's Model	RMS Method	Munse's Model				
				Beta	Weibull	Exponential	Rayleigh	Lognormal
B-19	130	94	253	136	176	6926	236	5087
B-23	165	119	207	173	231	9498	311	7197
B-14	1262	913	856	1326	2276	138117	3137	136322
B-21	814	596	499	885	1389	77487	1904	72237
B-10	1038	752	735	1091	1828	106847	2513	102819
B-1	1628	1178	735	1710	3029	193011	4188	196906
B-18	3144	2286	1341	3304	6348	458900	8849	509965
3-2	324	131	364	357	584	54186	829	67410
3-1	571	231	499	629	1157	119615	1604	163129
3-3	1500	607	782	1651	3712	461876	4943	744700
7-5	1278	517	714	1407	3068	369120	4113	579217
2-4	1930	781	900	2125	5031	659422	6631	1105680
5-4	1440	582	1092	1581	3534	437892	4715	696006

Table 17

Mean Fatigue Life Predictions for ASTM A588-A Butt Welds under SAE Bracket History and ASTM A36 Butt Welds under SAE Transmission History

Spec. No.	Life Predicted, blocks						
	Miner's Rule	Gurney's Model	Munse's model				
			Beta	Weibull	Exponential	Rayleigh	Lognormal
A588-A							
3	188	82	206	306	24631	426	27705
5	563	246	615	1084	115712	1535	160742
6	867	378	947	1785	213020	2545	321613
7	1019	444	1113	2151	267510	3073	416629
A36							
25-2	532	194	1316	1392	40627	860	244407
15-5	532	194	1316	1392	40627	860	244407
25-5	576	210	1426	1533	45359	945	281211
16-5	591	214	1457	1578	46957	972	293462
15-2	1168	426	2898	3577	123960	2164	969699
43-4	1168	426	2898	3577	123960	2164	969699
16-6	1168	426	2898	3577	123960	2164	969699
16-3	1168	426	2898	3577	123960	2164	969699
25-3	1168	426	2898	3577	123960	2164	969699
15-1	2661	965	6562	9623	400923	5699	4114519
43-6	2661	965	6562	9623	400923	5699	4114519
15-6	2661	965	6562	9623	400923	5699	4114519

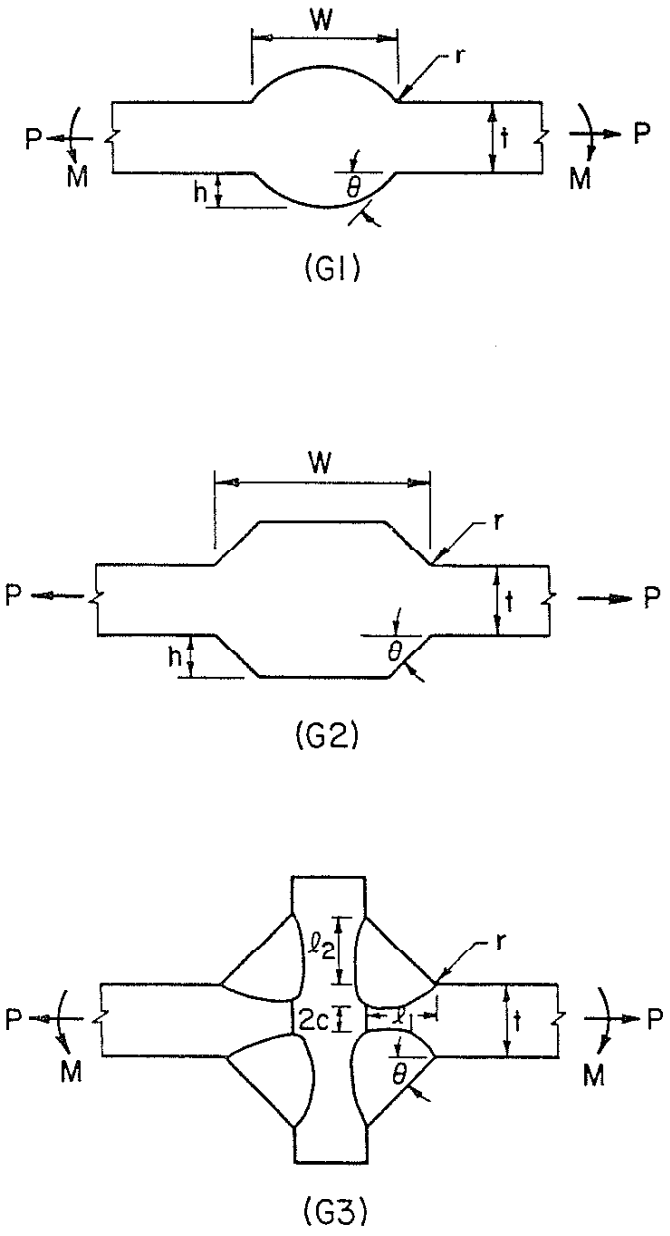

Fig. 1 Weldments Geometries.

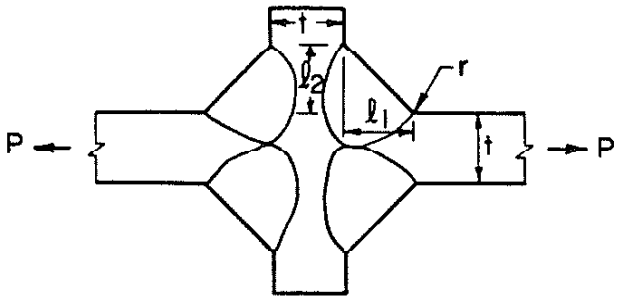

(G4)

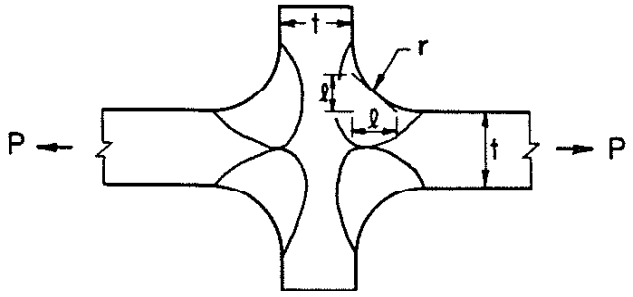

(G5)

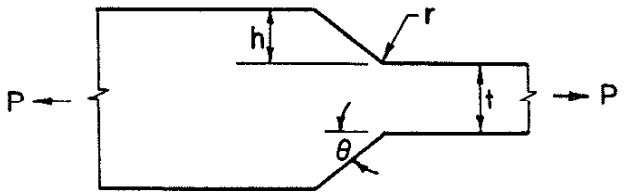

(G6)

Fig. 1 Continued.

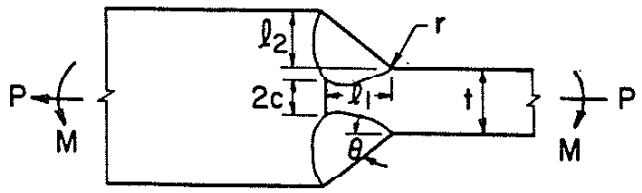

(G7)

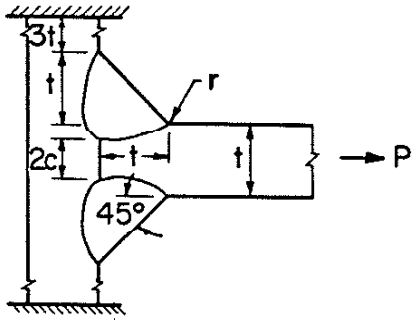

(G8)

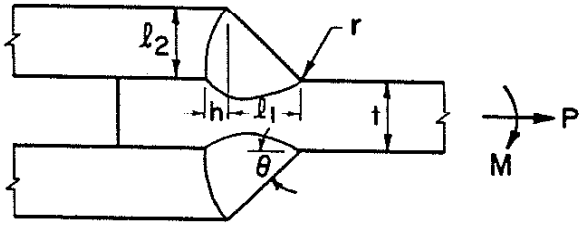

(G9)

Fig. 1 Continued.

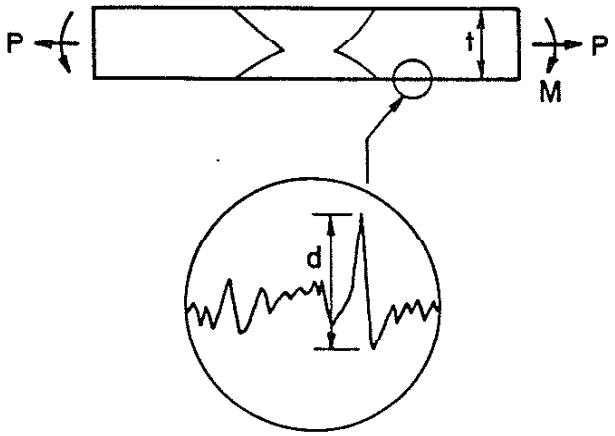

(G10)

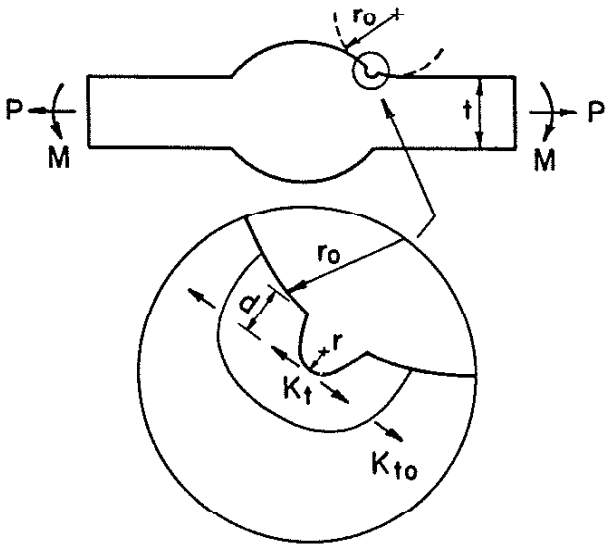

(G11)

Fig. 1 Continued.

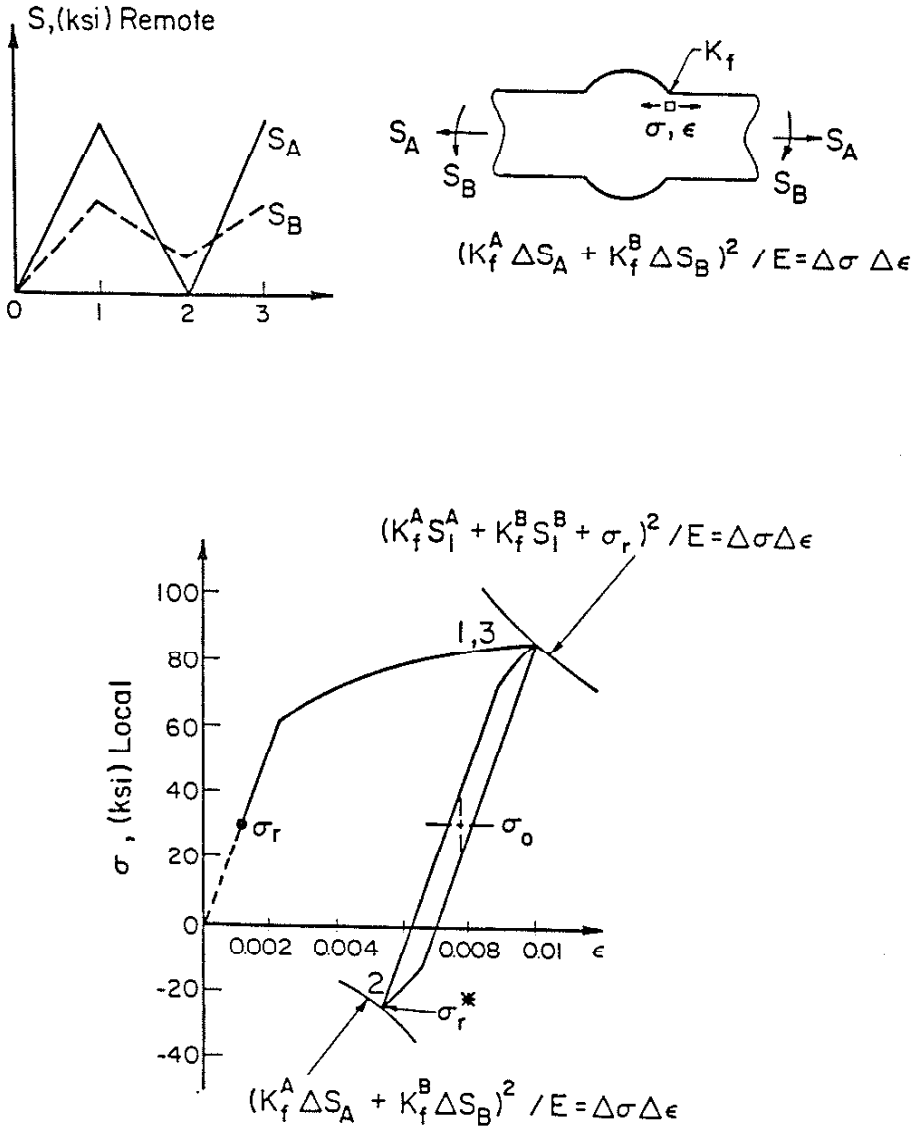

Fig. 2 Simulation of Local Stress-Strain Response at the Weld Toe with Tensile Residual Stress [6].

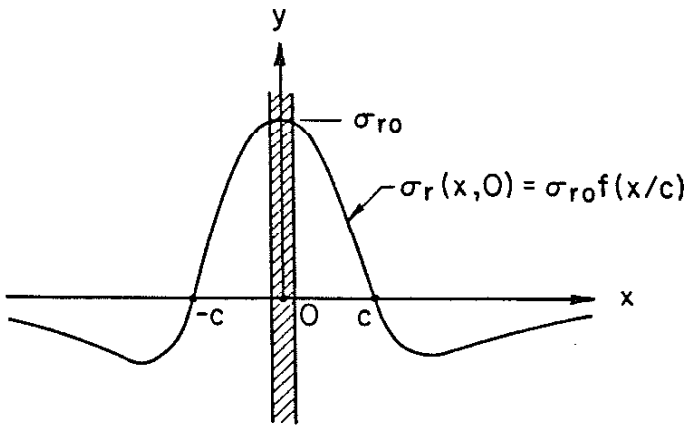

(A)

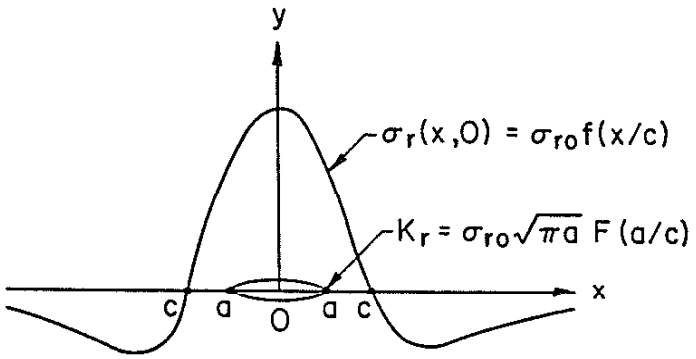

$$F(a/c) = \left\{ \frac{\left[1+(a/c)^4\right]^{1/2} - (a/c)^2}{1+(a/c)^4} \right\}^{1/2}$$

(B)

Fig. 3 (A) Longitudinal Residual Stress Field Duc to Welding (Hatched Area: Weld Metal).
(B) Crack in Residual Stress Field [18].

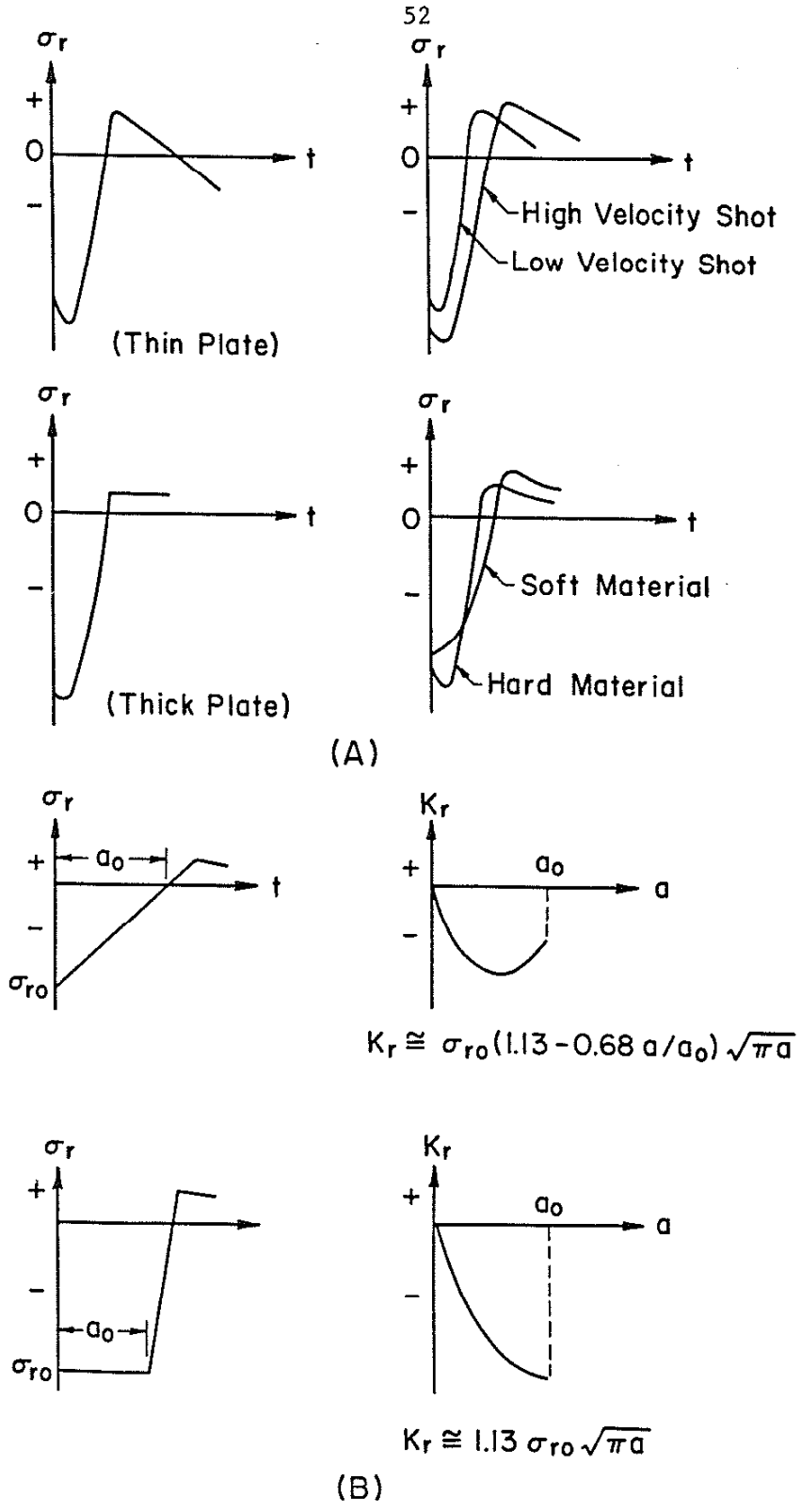

Fig. 4 (A) Typical Residual Stress Distribution Resulting from Shot-Peening [36].
(B) Hypothetical Notch Residual Stress Distribution and Corresponding Residual Stress Intensity Factors [21,22].

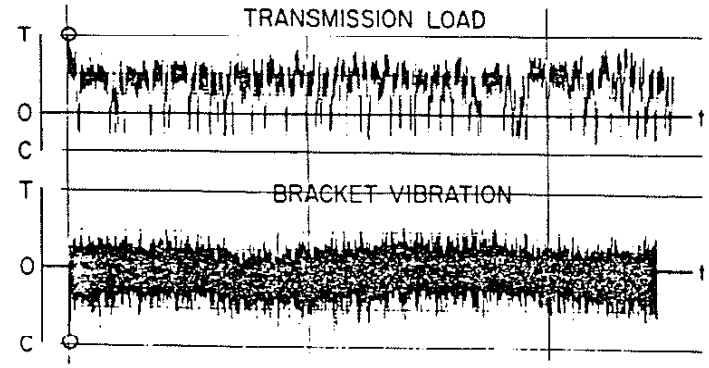

(A)

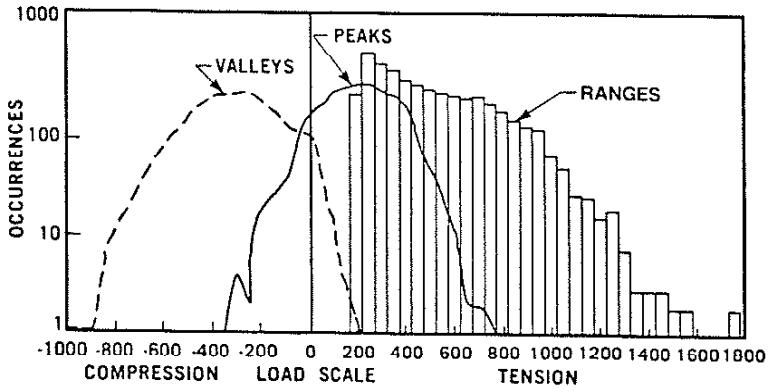

(B)

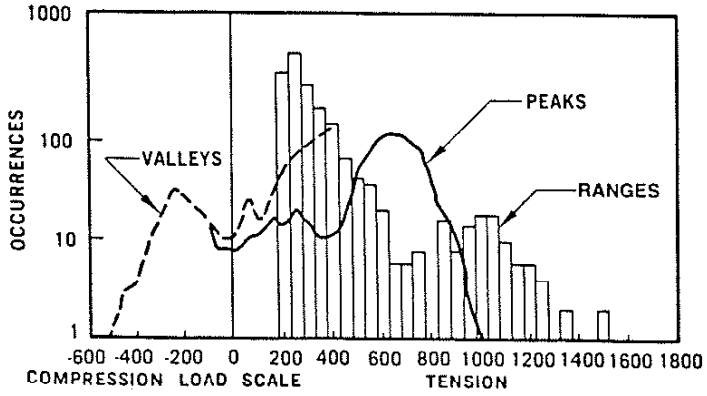

(C)

Fig. 5 (A) Load Amplitude-Time Display of the SAE Bracket and Transmission Histories.
(B) Bracket Histograms.
(C) Transmission Histograms [27].

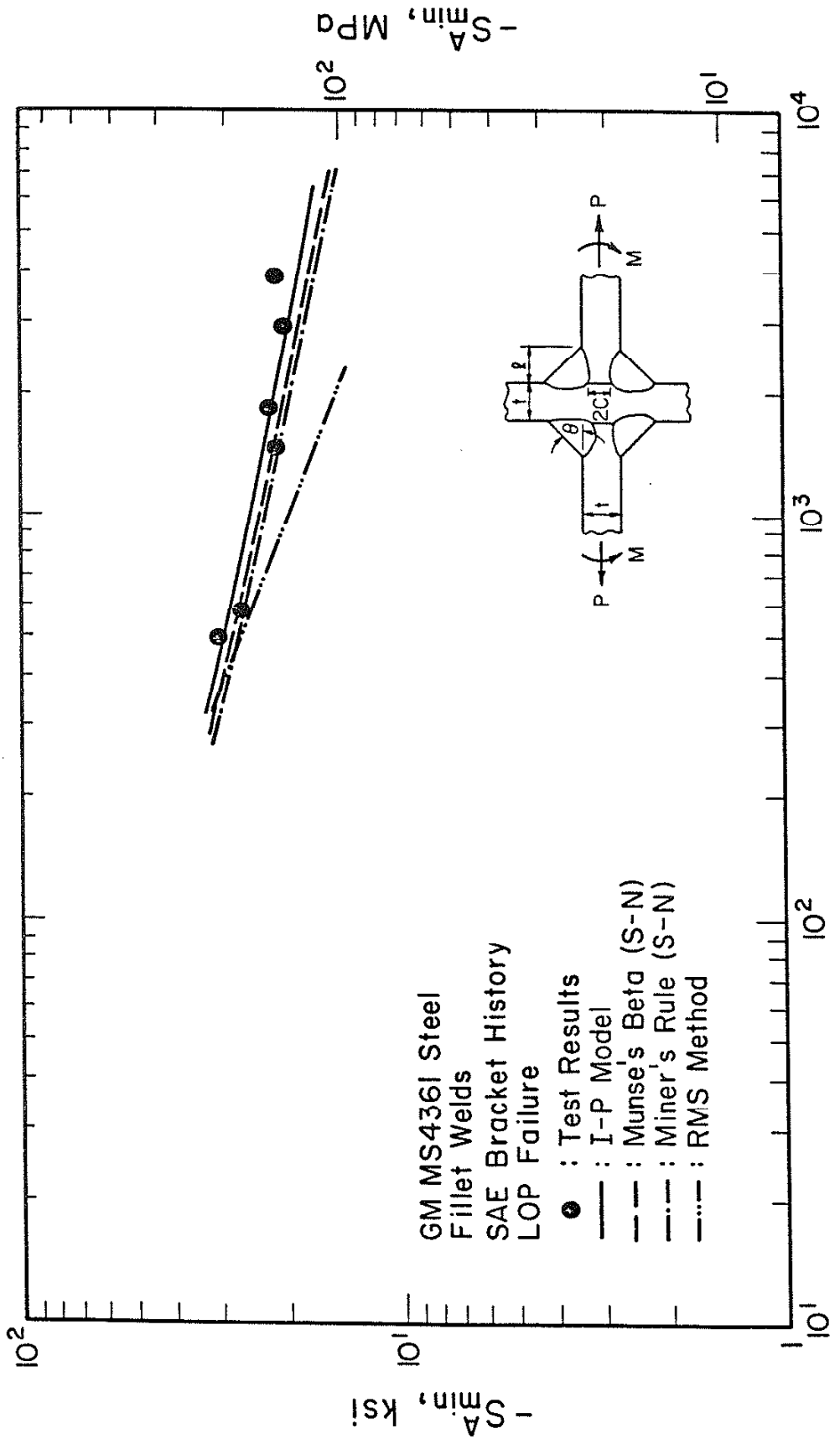

Fig. 6 Predictions and Test Results for MS4361 Cruciform Joints Subjected to SAE Bracket History.

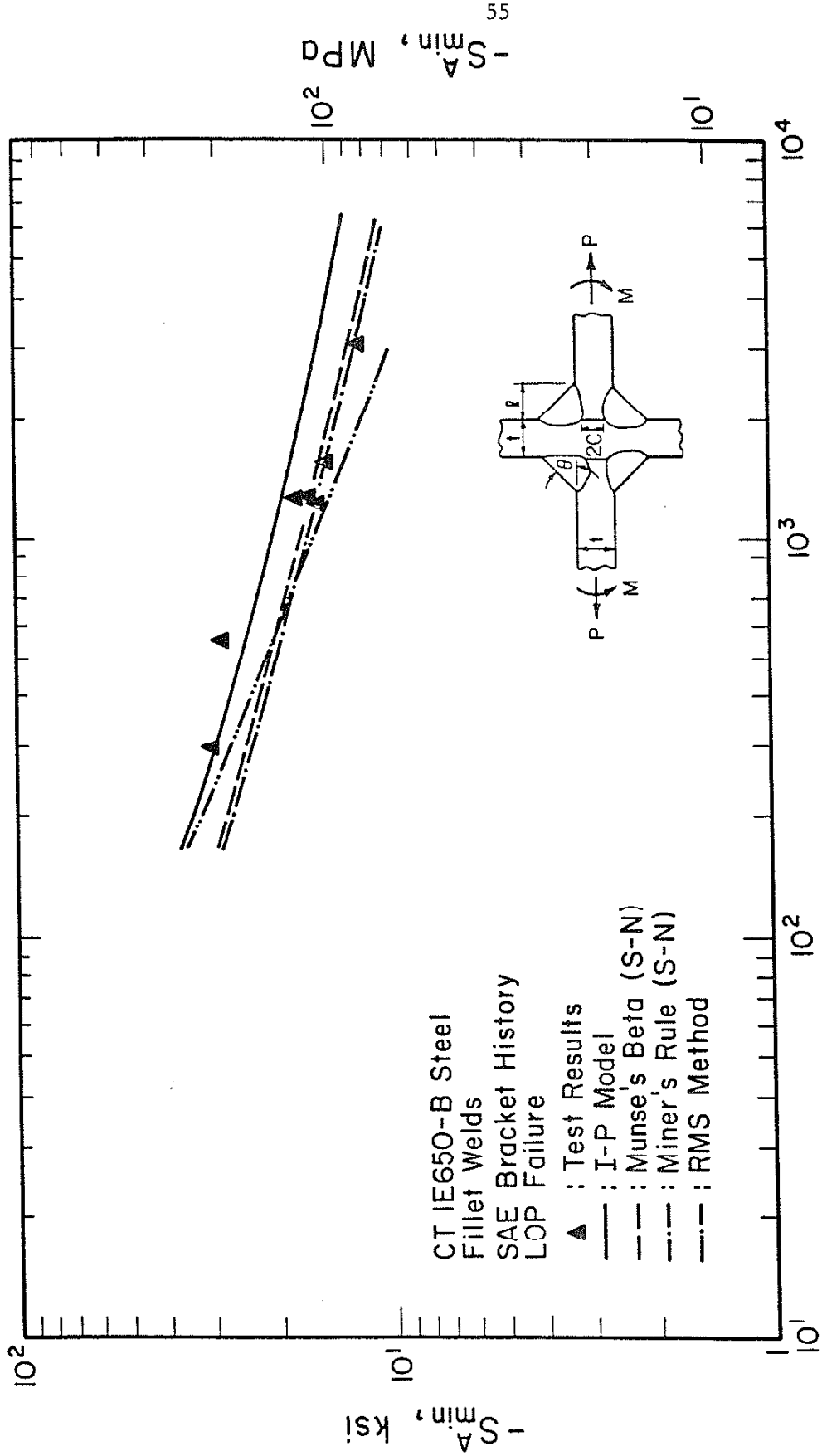

Fig. 7 Predictions and Test Results for 1E650-B Cruciform Joints Subjected to SAE Bracket History.

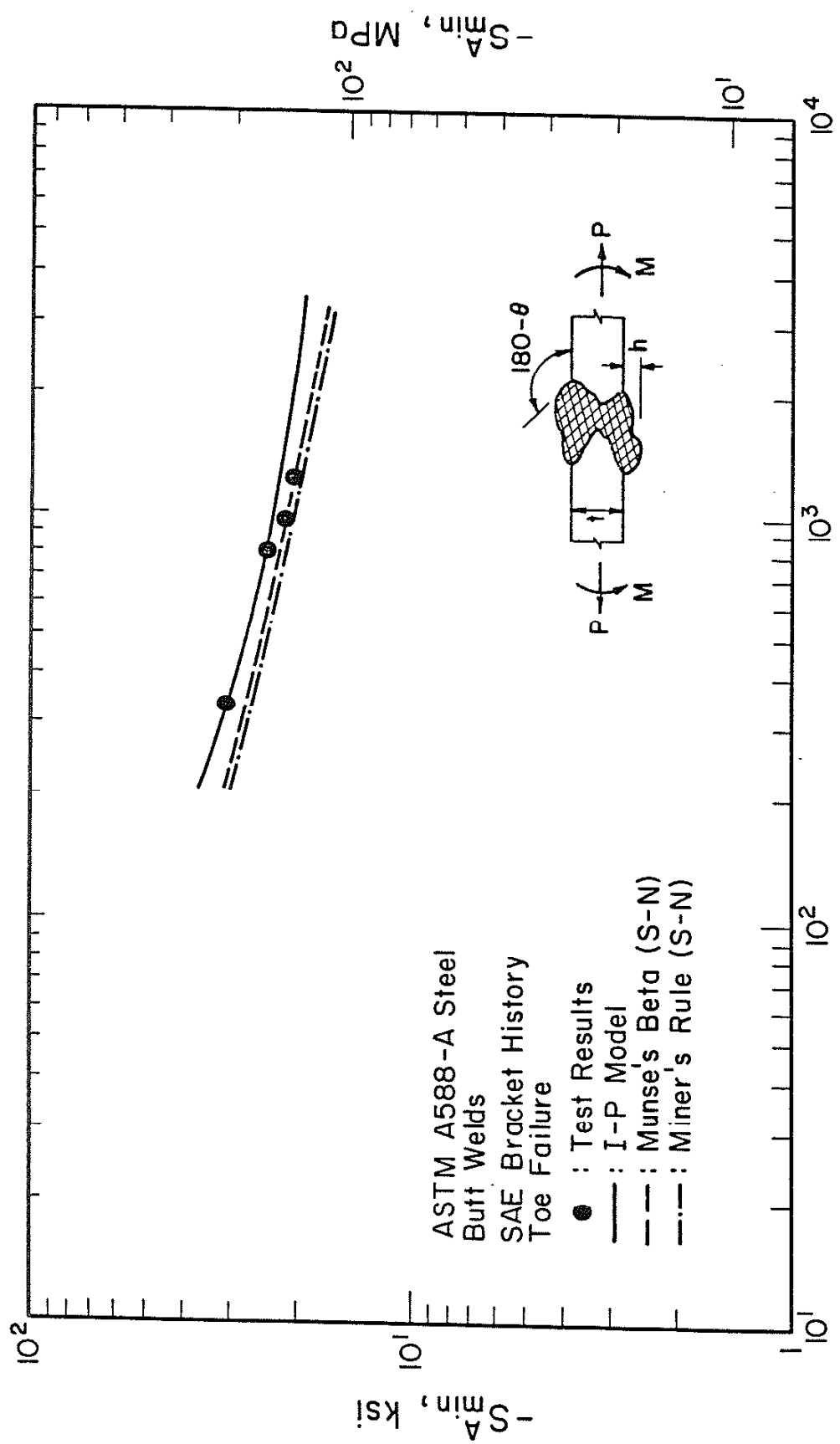

Fig. 8 Predictions and Test Results for ASTM A588-A Butt Welds Subjected to SAE Bracket History.

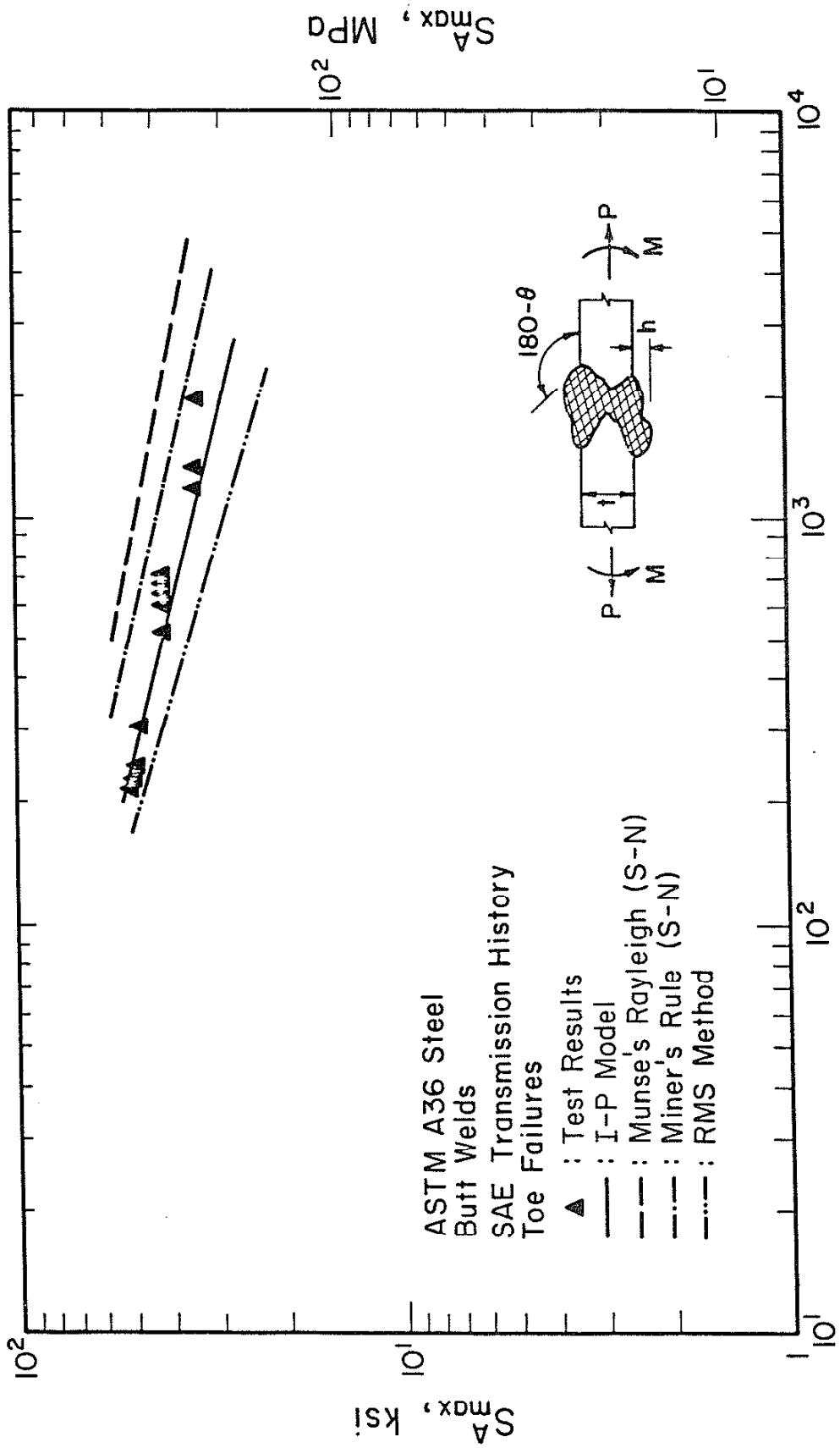

Fig. 9 Predictions and Test Results for ASTM A36 Butt Welds Subjected to SAE Transmission History.

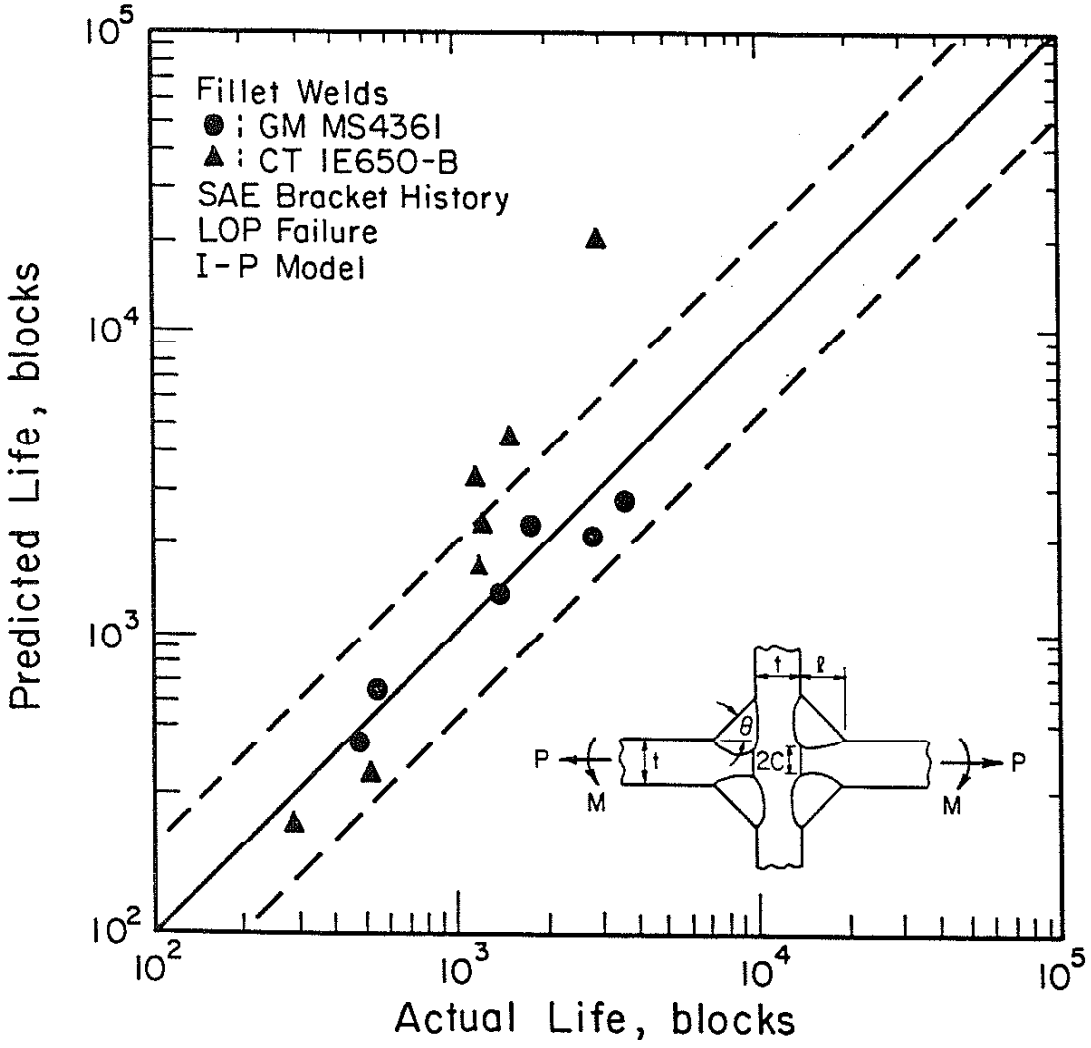

Fig. 10 Comparison of Predictions Made Using the I-P Model and Test Results for MS4361 and 1E650-B Cruciform Joints under SAE Bracket History.

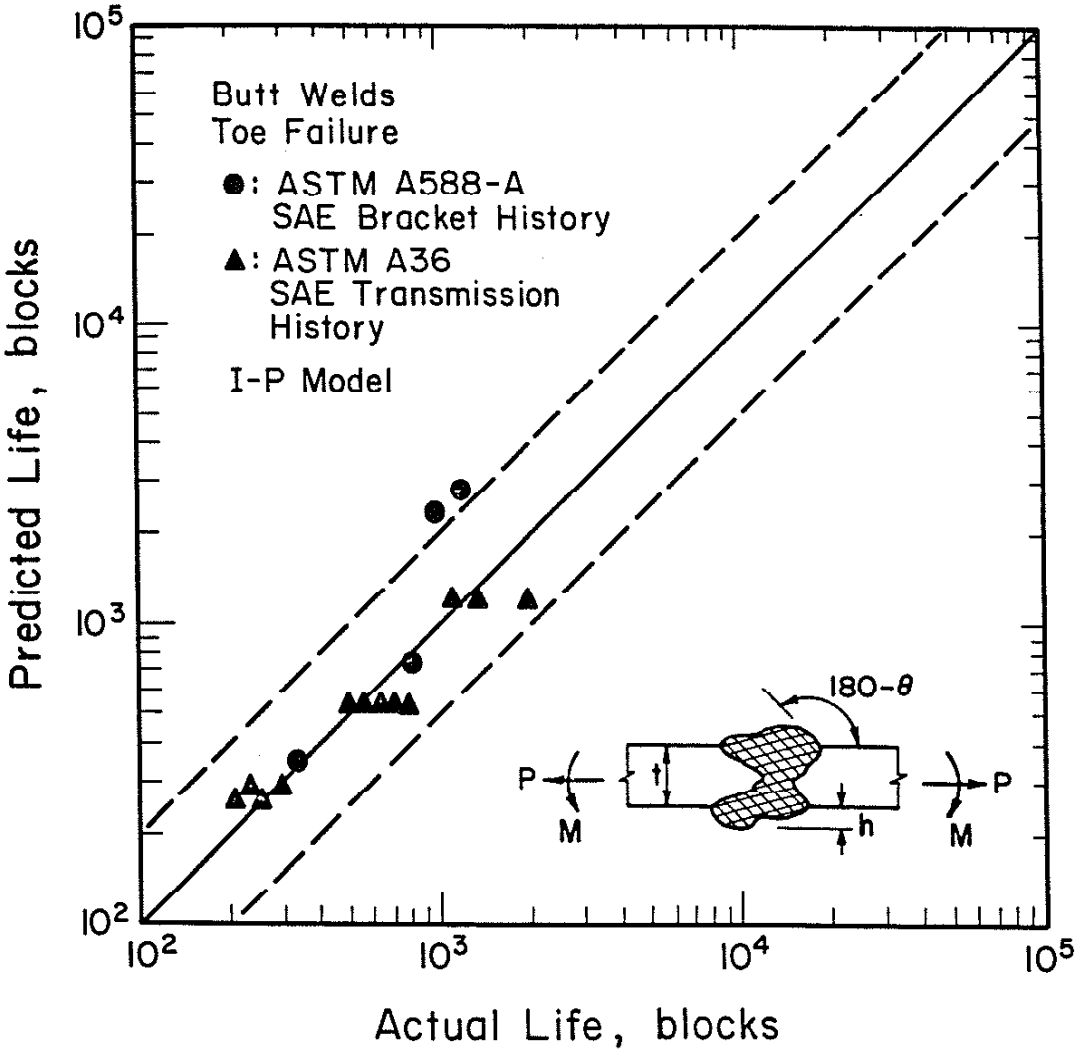

Fig. 11 Comparison of Predictions Made Using the I-P Model and Test Results for A588-A Butt Welds under SAE Bracket History and A36 Butt Weld under SAE Transmission History.

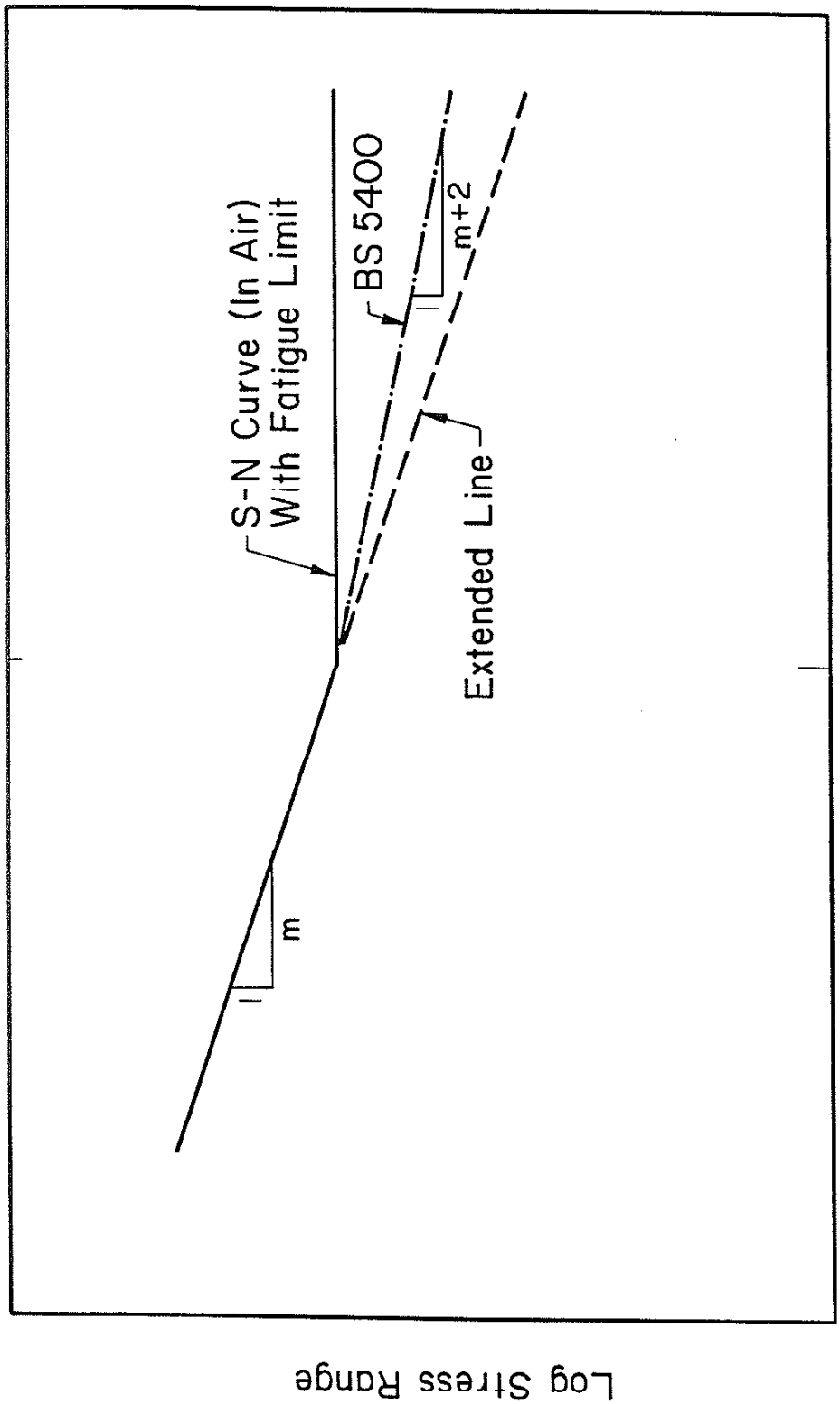

Fig. 12 Modification of the S-N Diagram.

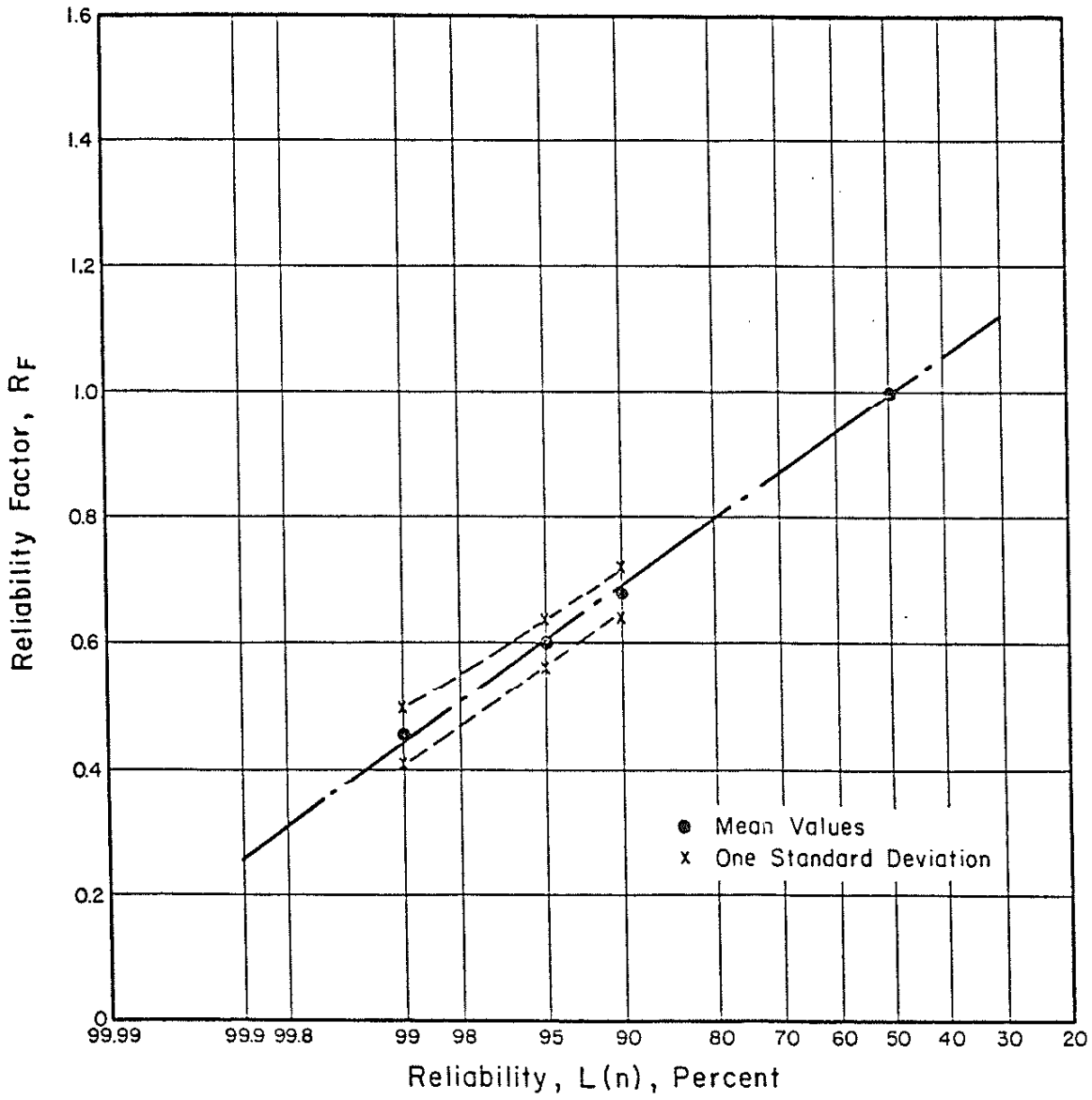

Fig. 13 Mean Values of Reliability Factor for Various Levels of Reliability [1].

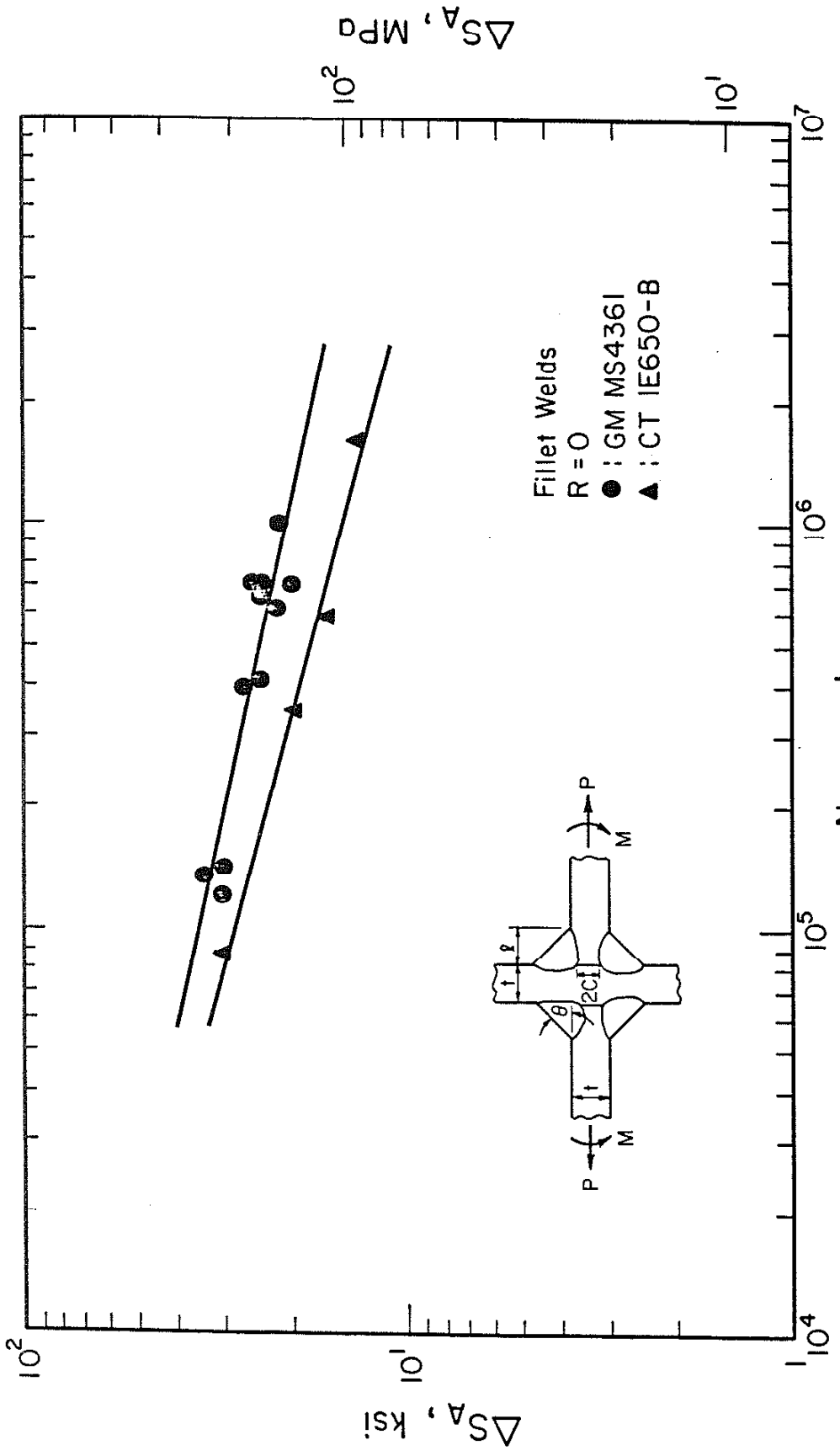

Fig. 14 Constant Amplitude Fatigue Test Results for MS4361 and 1E650 Cruciform Joints with Stress Ratio R = 0 [6].

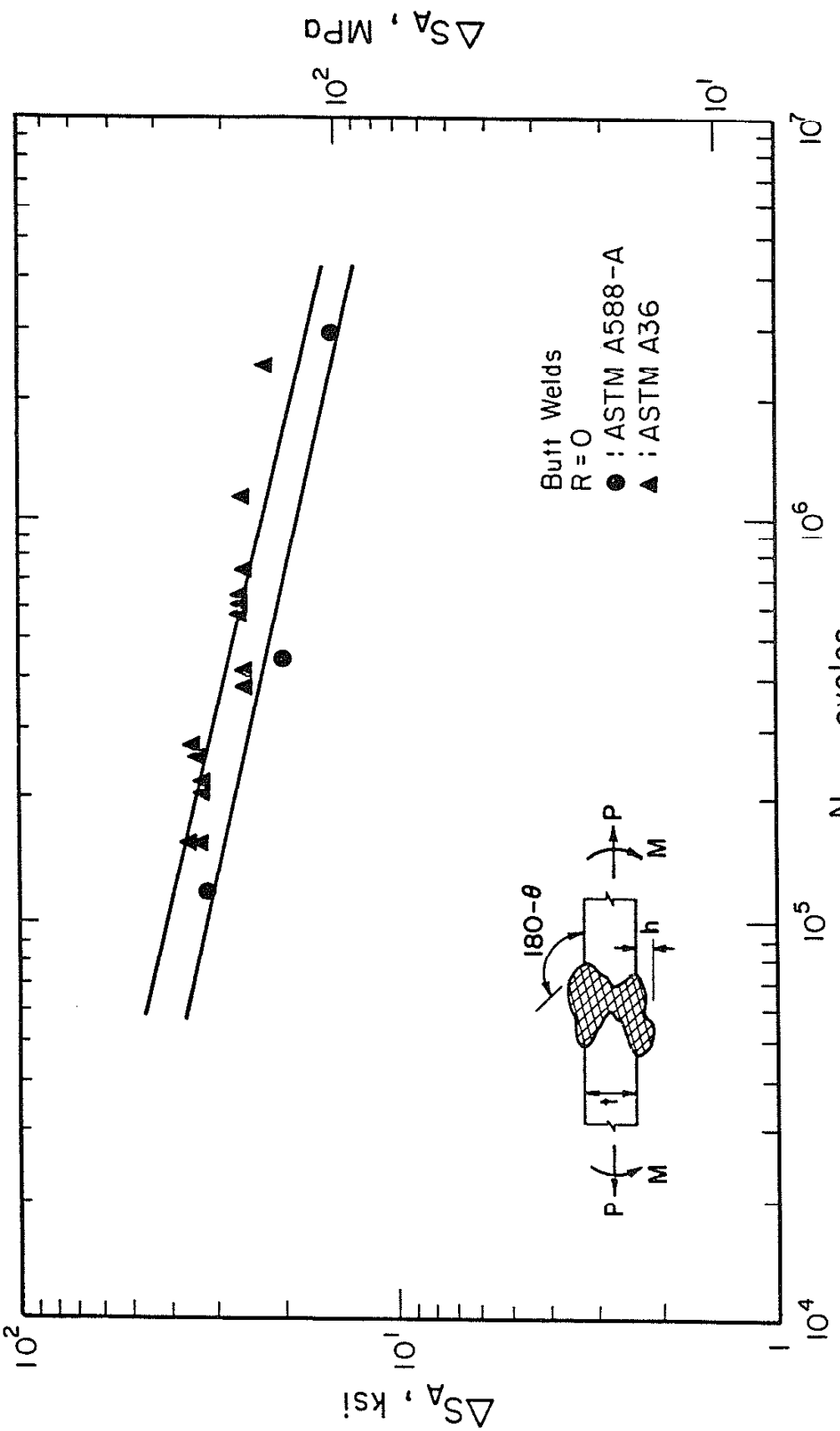

Fig. 15 Constant Amplitude Fatigue Test Results for A588-A and A36 Butt Welds with Stress Ratio R = 0 [25,35].

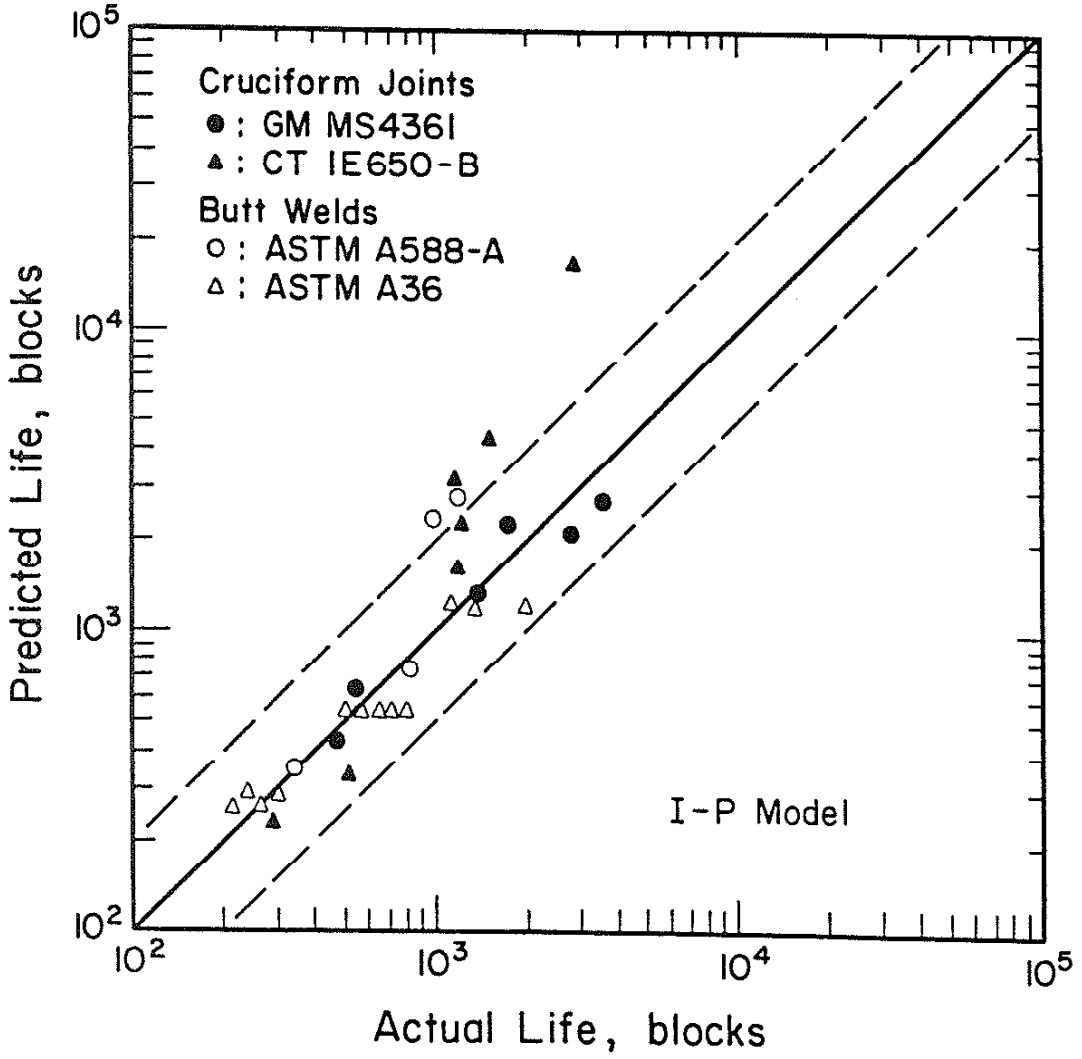

Fig. 16 Comparison of Actual and Predicted Fatigue Life Using the I-P Model.

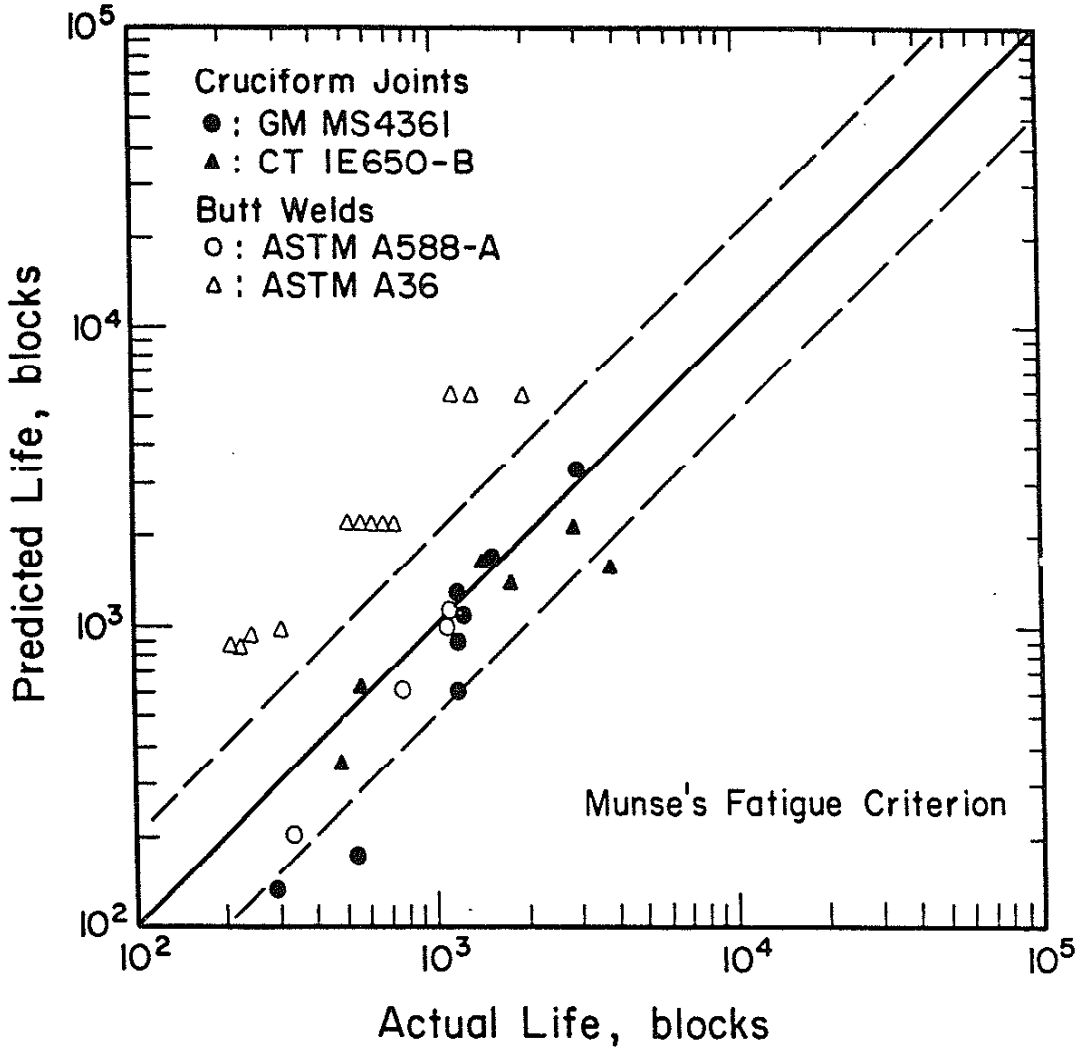

Fig. 17 Comparison of Actual and Predicted Fatigue Life Using Munse's Fatigue Criterion.

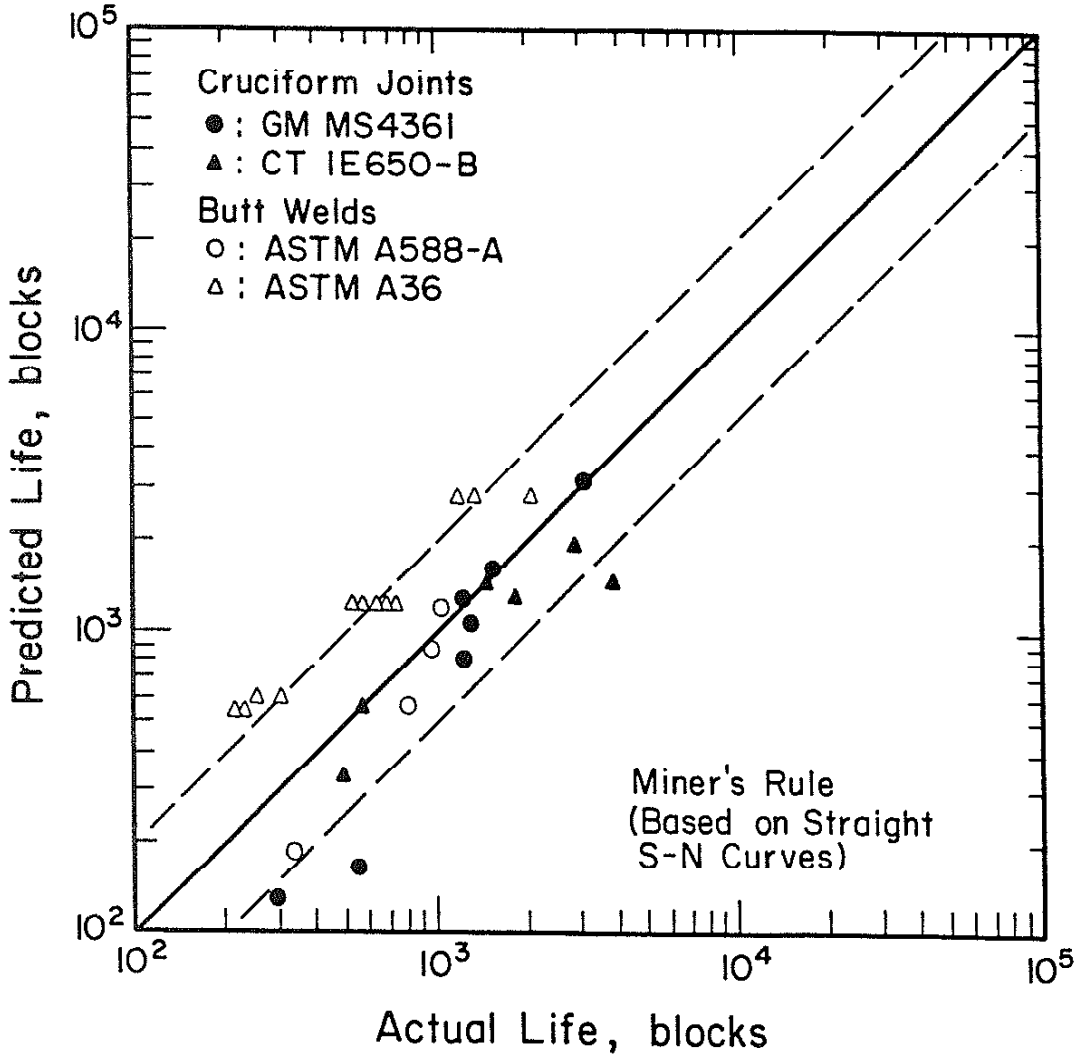

Fig. 18 Comparison of Actual and Predicted Fatigue Life Using Miner's Rule (Based on the Extended S-N Curve).

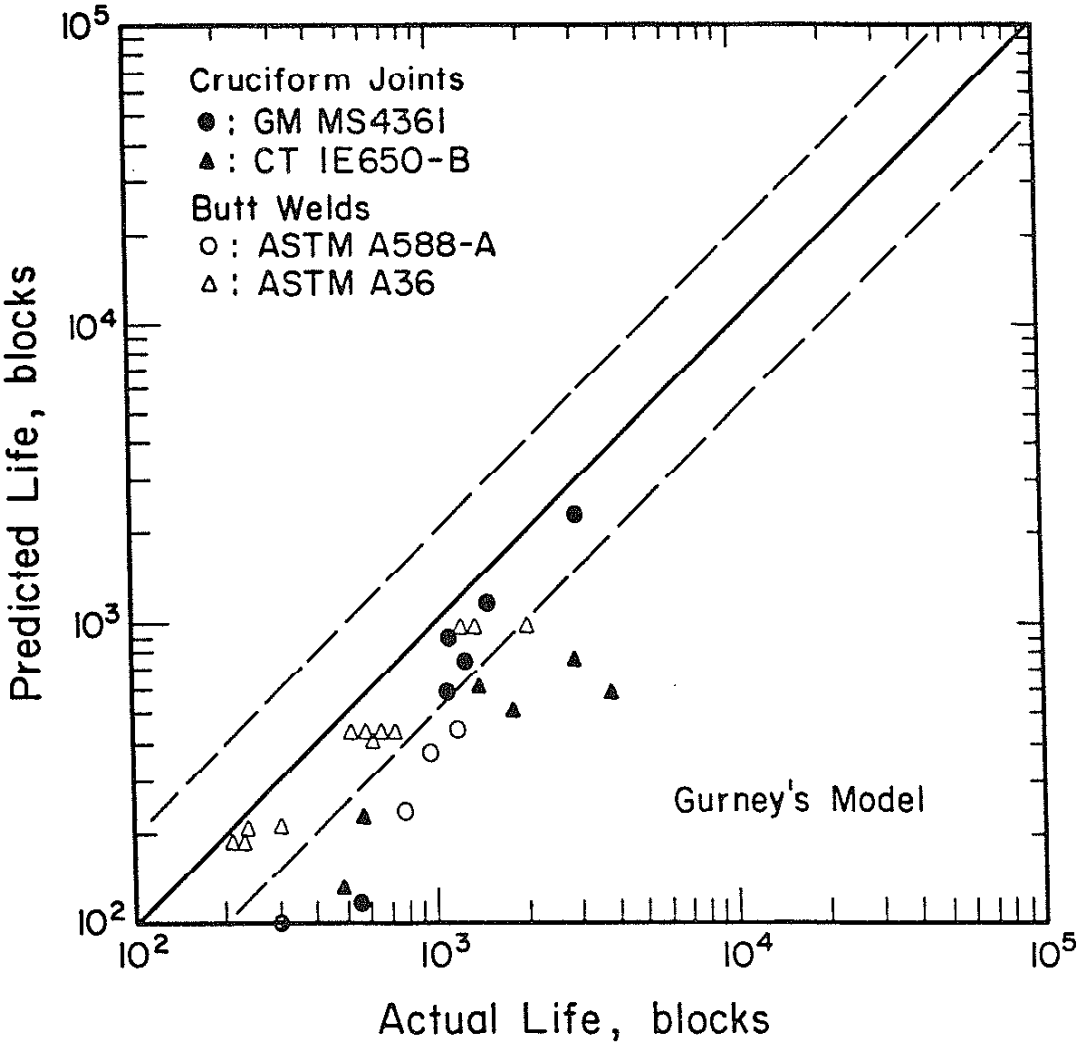

Fig. 19 Comparison of Actual and Predicted Fatigue Life Using Gurney's Model.

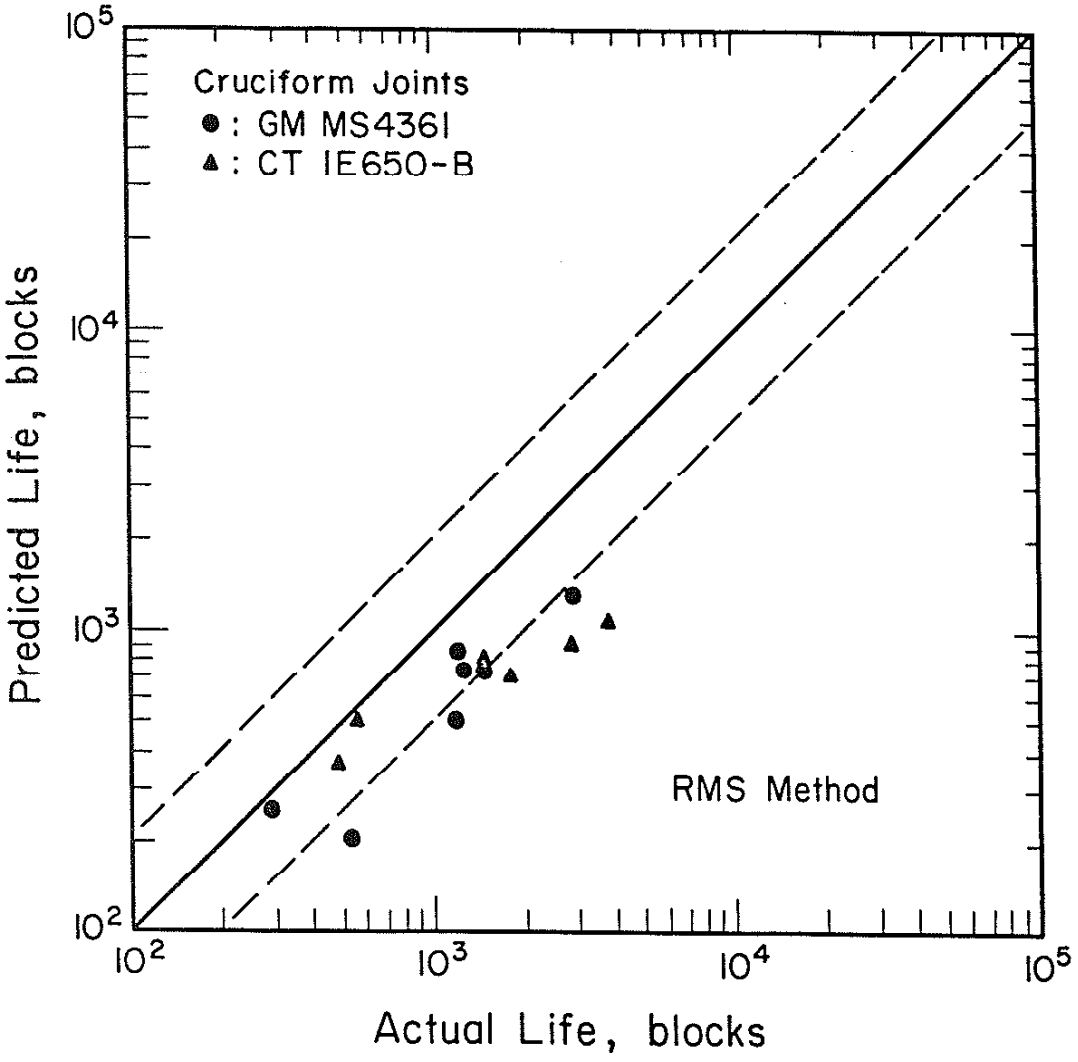

Fig. 20 Comparison of Actual and Predicted Fatigue Life Using the RMS Method.

Appendix A

STRESS INTENSITY FACTOR FOR THE SURFACE CRACK

An empirical equation for the stress intensity factor for a surface crack in a finite plate subjected to combined tension and bending loads has been proposed by Newman and Raju [30]:

$$K = (S_A + HS_B)\sqrt{\pi a/Q}\, F(a/t,\ a/c,\ c/w,\ \phi) \tag{A1}$$

where S_A and S_B = remotely applied tensile and bending stresses, as defined in Fig. A1.

a, t, c, w, ϕ = parameters characterizing the plate and crack geometry as defined in Fig. A2.

Q = crack shape factor for an elliptical crack.

$= 1 + 1.464(a/c)^{1.65}$, $(a/c < 1)$

for $0 < a/c \leq 1.0$, $0 \leq a/t < 1.0$, $c/w < 0.5$ and $0 \leq \phi \leq \pi$.

The functions F and H are defined so that the boundary-correction factor for tension is equal to F and the boundary-correction factor for bending is equal to the product of H and F as follows:

where
$$F = [M_1 + M_2(a/t)^2 + M_3(a/t)^4] f_\phi g f_w$$
$$M_1 = 1.13 - 0.09(a/c)$$
$$M_2 = -0.54 + 0.89/[0.2\ (a/c)]$$
$$M_3 = 0.5 - 1.0/[0.65+a/c]+14(1.0-a/c)^{24}$$
$$g = 1 + [0.1 + 0.35(a/t)^2](1 - \sin\phi)^2$$
$$f_\phi = [(a/c)^2\cos^2\phi + \sin^2\phi\ ]^{1/4}$$
$$f_w = [\sec(\ \pi c/w\sqrt{a/t}]^{1/2}$$

and

$$H = H_1 + (H_2 - H_1)\sin^p\phi$$

where

$$H_1 = 1 - 0.34a/t - 0.11(a/c)(a/t)$$

$$H_2 = 1 + G_1(a/t) + G_2(a/t)^2$$

$$G_1 = -1.22 - 0.12a/c$$

$$G_2 = 0.55 - 1.05(a/c)^{0.75} + 0.47(a/c)^{1.5}$$

$$p = 0.2 + a/c + 0.6a/t$$

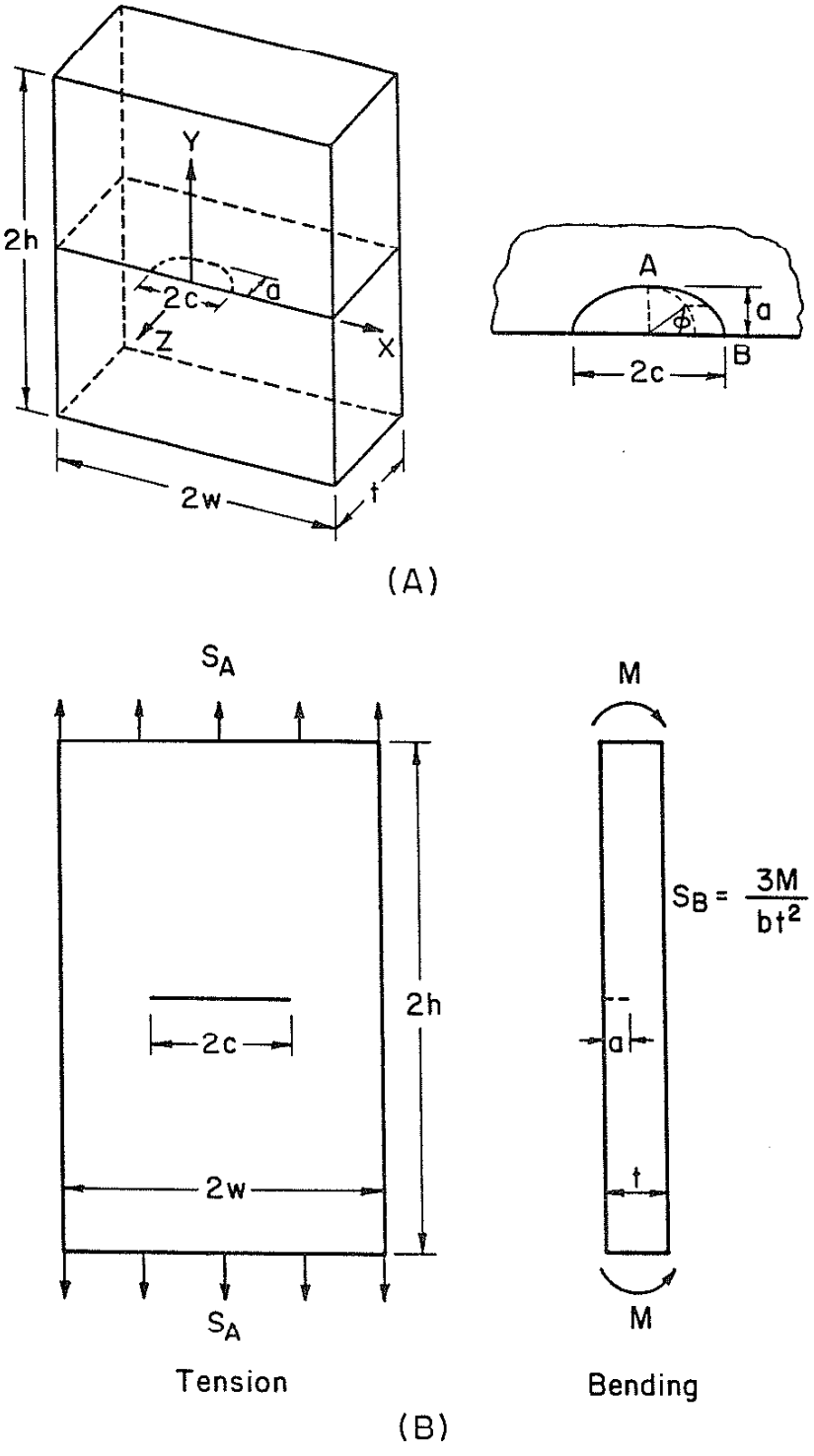

Fig. A1 (A) Surface Crack in a Finite Plate.
(B) Surface-Cracked Plate Subjected to Tension and Bending Load [30].

REFERENCES

1. Munse, W. H., Wilbur, T. W., Tellalian, M. L., Nicoll and Wilson, K., 'Fatigue Characterization of Fabricated Ship Details for Design,' SSC-318, Ship Structure Committee, 1983.

2. Gurney, T. R. , 'Some Fatigue Tests on Fillet Welded Joints under Simple Variable Amplitude Loading,' The Welding Institute, May 1981.

3. Zwerneman, F. J., 'Influence of The Stress Level of Minor Cycles on Fatigue Life of Steel Weldments,' Department of Civil Engineering, The University of Texas at Austin, Master's Thesis, May 1983.

4. Maddox, S. J., 'A Fracture Mechanics Approach to Service Load Fatigue in Welded Structures,' Welding Research International Vol. 4, No. 2, 1974.

5. Schilling, C. G., Klippstein, K. H., Barsom, J. M. and Blake, G. T., 'Fatigue of Welded Steel Bridge Members under Variable Amplitude Loadings,' NCHRP Project Final Report 12-12, Aug. 1975.

6. Ho, N. J. and Lawrence, F. V., 'The Fatigue of Weldments Subjected to Complex Loadings,' FCP Report No. 45, College of Engineering, University of Illinois at Urbana-Champaign, Jan., 1983.

7. Turmov, G. P., 'Determining the Coefficient of Concentration of Stress in Welded Joints,' Avt. Svarka, No. 10, 1976, pp. 14-16.

8. Heywood, R. B., 'Designing by Photoelasticity,' Chapman and Hall Ltd., 1952. Nishida, M., 'Stress Concentration,' Morikita Pub. Co. Ltd., 1967.

9. Bakshi, O. A., Zaitsev, N. L. and Shron, L. B., 'Effect of the Geometry of Fillet Welded Joints on Stress Concentration Factors and Stress Gradient in Welds,' Svar. Proiz., No. 8, 1982, pp. 3-5.

10. Hibbitt, Karlsson and Sorenson, Inc., Providence, RI, 1980.

11. Lawrence, F. V., Mattos, R. J., Higashida, Y., Burk, J. D., 'Estimation of Fatigue Crack Initiation Life of Weld,' ASTM STP 648, American Society of Testing and Materials, 1978, p. 420.

12. Peterson, R. E., 'Notch Sensitivity,' Metal Fatigue, Chap. 13, Sines and Waisman (ed.) McGraw-Hill, New York, 1959.

13. Dowling, N. E., 'Fatigue Life Prediction for Complex Load Versus Time Histories,' Transactions of the ASME, Vol. 105, 1983, pp. 206-214.

14. Dowling, S. D. and Socie, D. F., 'Simple Rainflow Counting Algorithms,' International Journal of Fatigue, Vol. 4, No. 1, 1982.

15. Paris, P. C. and Erdogan, F., 'A Critical Analysis of Crack Propagation Law,' Journal of Basic Engineering, ASME Trans., Vol. 85, Ser. D. No. 4. 1963. p. 528.

16. Elber, W., 'The Significance of Fatigue Crack Closure,' ASTM STP 495, American Society for Testing and Materials, 1971.

17. Maddox, S. J., 'An Analysis of Fatigue Cracks in Fillet Welded Joints,' International Journal of Fracture, Vol. 11, No. 2, 1975, pp. 221-243.

18. Tada, H. and Paris, P. C., 'The Stress Intensity Factor for a Crack Perpendicular to the Welding Bead,' International Journal of Fracture, Vol. 21, 1983, pp. 279-284.

19. Smith, I. .F. .C. and Smith, R. A., 'Fatigue Crack Growth in a Fillet Welded Joint,' Engineering Fracture Mechanics, 1983.

20. Nelson, D. V. and Socie, D. F., 'Crack Initiation and Propagation Approaches to Fatigue Analysis,' ASTM STP 761, 1982, pp. 110-132.

21. Throop, J. F., 'Fracture Mechanics Analysis of the Effects of Residual Stress on Fatigue Life,' Journal of Testing and Evaluation, Vol. 11, No. 1, Jan. 1983, pp. 75-78.

22. Elber, W., 'Fracture Toughness Testing and Slow Stable Cracking,' ASTM 559, American Society for Testing and Materials, 1974, pp. 45-58.

23. Socie, D. F., 'Estimating Fatigue Crack Initiation and Propagation Lives in Notched Plates under Variable Loading History,' TAM Report No. 417, University of Illinois, Urbana-Champaign, 1977.

24. Fash, J. W. and Socie, D. F., 'Fatigue Life Predictions for Long History,' Department of Mechanical and Industrial Engineering, University of Illinois at Urbana-Champaign, Feb. 1982.

25. Deves, T. J., Kurath, P., Sehitoglu, H., and Morrow, J., 'The Effect of Selected Subcycle in Block Loading Fatigue Histories,' FCP Report No. 42, College of Engineering, University of Illinois at Urbana-Champaign, Mar. 1982.

26. Prine, D. W., Maline, V. D., Yung, J.-Y., McMahon, J. and Lawrence, F. V., 'Improved Fabrication and Inspection of Welded Connections in Bridge Structures,' Federal Highway Administration, U.S. Department of Transportation, Report No. FHWA/RD-83/006, 1983.

27. Wetzel, R. M., editor, 'Fatigue under Complex Loading: Analysis and Experiments,' Advances in Engineering, Vol. 6, SAE, 1977.

28. Higashida, Y. and Lawrence, F. V., 'Strain Controlled Fatigue Behavior of Weld Metal and Heat-Affected Base Metal in A36 and A514 Steel Welds, FCP Report No. 22, College of Engineering, University of Illinois at Urbana-Champaign, Aug. 1976.

29. Frank, K. H., 'The Fatigue Strength of Fillet Welded Connections,' Ph.D. Thesis, Lehigh University, 1971.

30. Newman, J. C. and Raju, I. S., 'An Empirical Stress-Intensity Factor for the Surface Crack,' Engineering Fracture Mechanics, Vol. 15, No. 1-2, 1981, pp. 185-192.

31. Schilling, C. G. and Klippstein, K. H., 'Fatigue of Steel Beams by Simulated Bridge Traffic,' Journal of Structural Division, Proceedings of ASCE, Vol. 103, No. ST8, Aug. 1977.

32. BS5400: Part 10: 1980 'Steel, Concrete and Composite Bridges, Code of Practice of Fatigue.'

33. Hudson, C. M., 'A Root-Mean-Square Approach for Predicting Fatigue Crack Growth under Random Loading,' ASTM STP 748, 1981, pp. 41-52.

34. Stefaniuk, A. R., 'Fatigue Behavior of Butt Welded Joints under a Random Loading,' Department of Civil Engineering, University of Illinois at Urbana-Champaign, May 1975.

35. Gurney, T. R., 'Fatigue of Welded Structures,' 2nd Edition, Cambridge University Press, 1979.

36. Al-Hassani, S. T. S., 'The Shot Peening of Metals - Mechanics and Structures,' SAE Report No. 821452.

37. Chang, S.-T. and Lawrence, F. V., 'Improvement of Welded Fatigue Resistance,' FCP Report No. 46, University of Illinois at Urbana-Champaign, College of Engineering, Jan. 1983.